2020

Synthesis of multifunctional nanoparticles for imaging and enhancement in therapy

Gabrielle Seymore

Synthesis of multifunctional nanoparticles for imaging and enhancement in therapy

A thesis submitted in partial fulfillment of the requirements
for the degree of Master of Science at Virginia Commonwealth University.

By
Gabrielle Pierson Seymore
Bachelor of Science in Physics, College of Charleston, May 2018

Advisor: Jessika V. Rojas
Assistant Professor, Department of Mechanical and Nuclear Engineering

Virginia Commonwealth University
Richmond, VA
May, 2020

ACKNOWLEDGEMENTS

I would like to thank my advisor Dr. Rojas for her continuous advice and encouragement throughout the course of this project and her willingness to collaborate. I would also like to thank the entire Department of Radiation Oncology and the faculty within the Division of Medical Physics. Their teaching and hard work has prepared me very well for an exciting career. Finally, I would like to thank my family for their unwavering support and patience over the past few years. Thank you.

Table of Contents

List of Tables

List of Figures

Abstract

SYNTHESIS OF MULTIFUNCTIONAL NANOPARTICLES FOR THE POTENTIAL USE IN RADIATION THERAPY TREATMENT AND IMAGING MODALITIES

By Gabrielle P. Seymore, B.S.
A thesis submitted in partial fulfillment of the requirements for the degree of Master of Science at Virginia Commonwealth University.

Virginia Commonwealth University, 2020.

Major Director: Jessika V. Rojas, Assistant Professor, Department of Mechanical and Nuclear Engineering

The purpose of this work was to synthesize nanoparticles composed of high atomic number elements and semiconductor material in a core/shell structure for the potential to be used as enhancers for radiotherapy as well as luminescence imaging platforms. Additionally, to quantify their role in free radical production after exposure to ionizing radiation through chemical routes. Spherical gold nanoparticles were synthesized via a citrate stabilizer method. Two sizes of 12nm and 25 nm gold spheres were used as the cores for the europium-doped gadolinium vanadate flower-shaped shell. The production of 7-hydroxycoumarin-3-carboxylic acid in an aqueous environment upon kV irradiation of its precursor, coumarin-3-carboxylic acid, was assessed and used as a fluorescence detector for hydroxyl radicals. The quantification of excess or moderation of hydroxyl radicals in the presence of the nanomaterial as compared to a control sample can

indicate the potential for increased DNA damage for purposes such as tumor control. This work indicates the potential for physical and chemical enhancement in the presence of nanomaterials.

I. Introduction

Radiation Therapy and Limitations

Radiation therapy is used in the treatment of approximately 50% of all cancer patients, both as a primary or adjuvant treatment avenue[1]. It has various roles in the care process for each individual patient ranging from pre and post-surgical radiation, concomitant chemotherapy, total body irradiation in preparation for bone marrow transplant, palliation, and much more. Due to the steady prevalence of cancer incidence and the successes of radiation oncology in the past, the field has advanced in recent years due to new modalities and delivery techniques. However, despite recent advancements in all aspects of the radiotherapy process, radiation still cannot discriminate between healthy and diseased tissues, therefore creating limitations of its success[2].

Standard radiation therapy delivers ionizing radiation with an external megavoltage beam to a specified site of the body that is believed to contain cancerous cells via a linear accelerator ("linac"). Due to the traversing of the beam through skin and associated normal tissue, all objects within the beam path can be affected by the treatment. Megavoltage photon beams generated via linac have an associated skin-sparing effect with higher energies and can deliver maximum achievable dose to deep-seated tumors with less dermatitis and undesirable skin effects. While energy improvements, multi-leaf collimators (MLCs), and intensity-modulated radiation therapy (IMRT) have contributed to conformance to tumor volumes and improved targeting, many patients still experience normal tissue toxicity. Normal tissue toxicity can lead to various serious and uncomfortable side effect for patients dependent upon if the affected tissue is acute or late responding. These may include nausea, vomiting, diarrhea, pain, pneumonitis, chronic fibrosis, and more[3]. Additionally, tendencies are present to be conservative with dose prescriptions due to the proximity of critical structures and organs at risk (OAR) which can influence the clinical outcome for the patient[4].

Nanotechnology in medicine

Nanoparticles have been explored for many applications in medicine including drug delivery, hyperthermia, diagnosis, and imaging[5]. Nanotechnology is also one proposed solution to concentrating damage to cancerous cells while sparing normal tissue, by taking advantage of the

therapeutic window and inducing different responses between healthy and diseased tissues for clinical advantage[3]. The theory proposes introducing inorganic material into the body to interact with the ionizing radiation being delivered in order to "sensitize" the spatial locations where the nanomaterial is present. Therefore, this may contribute to achieving the clinical goal without escalating the dose and risking the critical structures and normal tissue in proximity. These materials have also been referred to in the literature as nano-radio-enhancers (NRE) to distinguish them from radiosensitizing drugs that inhibit DNA repair, but effectively cover the same subject matter[5]. In order to investigate the success and increased efficiency of this proposed treatment, the interactions of the nanomaterial with the ionizing radiation as well as the interactions of the nanomaterial with the body itself must be considered. Dose enhancement has been investigated by multiple research groups over the years due to the lack of understanding of the mechanisms for enhancement and discrepancies in predictive models for dose deposition and experimental results[1].

Nanomaterial influence on the principles of radiotherapy

It is first imperative to understand the basis of radiotherapy before examining the effect nanomaterial could have on these mechanisms. The principles of radiation therapy are based on the 5 R's of radiobiology: repair, reoxygenation, redistribution, repopulation, and radiosensitivity. The presence of nanomaterial contributes to these pillars and influences their role in effective cancer treatment. Cui et al. review and summarize each of these R's and analyze the nanomaterial impact of them[1].

1) Repair: DNA damage is the goal and result of traditional radiotherapy, and is sought to be amplified in the presence of nanoparticles. Not only is the physical damage effective, but also inhibiting or disrupting the intrinsic repair mechanisms of the cells could lead to increased cell death. Reactive Oxygen Species (ROS) scavenging is a repair pathway that attempts to remove those generated radicals post-irradiation, however cells in oxidative stress have limited scavenging capabilities which has been demonstrated in the presence of silver nanoparticles (AgNP).
2) Reoxygenation: Oxygen is considered radiotherapy's greatest natural radiosensitizer. While many creative tools have been utilized to reduce hypoxia, including specific chemotherapy drugs and fractionation schemes capitalizing on reoxygenation after

treatment, there is little evidence that demonstrates nanomaterial reoxygenates tumor sites. The oxidative state of the tumor during irradiation influences the effective radiosensitization by the nanomaterial. Consequently, nanomaterial appears to perform best under oxia, or normal oxygen levels of the cells.

3) Redistribution: The phases of the cell cycle all have associated radiosensitivity. While it would seem advantageous to redistribute tumor cells into the most sensitive phases G_2/M for treatment, conflicting evidence exists to support if nanomaterial affects this redistribution. Another method pertaining to redistribution is the use of cell cycle checkpoints. Checkpoints exist between the cell phases to screen and repair abnormal cells if these checkpoints are damaged or down-regulated then cell death could occur. Cell cycle synchronization has been demonstrated by multiple groups, although more in vivo studies are needed to confirm this concept.
4) Repopulation: Repopulation refers to the proliferation of cells, healthy and diseased, after irradiation. While it is advantageous for affected normal tissue of radiotherapy to proliferate and replace itself, repopulation is also responsible for maintained tumor presence or growth. Prevention of repopulation includes halting angiogenesis and production of factors such as vascular endothelial growth factor (VEGF). When considering the use of nanomaterial, repopulation effects will change the local concentrations of nanoparticles due to the evolving ratios and excretion over time. Therefore special dosing considerations and fractionation schemes must be considered based on the specific proliferation time of the tumor site involved.
5) Radiosensitization: This principle of radiobiology refers to the intrinsic radiosensitivity of cells. Due to heterogeneous mixtures of cells within tumor volumes, this cannot be solely defined by one value. It is essential to identify that nanomaterial as radiosensitizers refer to increased dose deposition locally, not aiming to modify the inherent nature of the cell itself. Survival fraction is often the measure of radiosensitivity. While decreased survival fractions have been observed in the presence of nanomaterial, no correlation has been demonstrated between nanomaterial and intrinsic radiosensitivity. Additionally, radiosensitizers have been considered for radioresistant tumors specifically to enhance the treatment effectively.

Nanomaterial influence on photon interactions and free radical production

To further understand how nanomaterial interacts with the body and ionizing radiation, photon interaction mechanisms with matter must also be examined. Three main interactions of radiation with matter exist in radiation oncology. This work will primarily focus on photon interactions relevant to this research. Photoelectric effect, Compton scatter, and pair production are the primary photon interactions relevant to radiation therapy. While Compton scatter dominates for most of the megavoltage range, pair production is possible once the threshold of 1.022 MeV is surpassed. The photoelectric cross-section (α) increases proportionally with $(Z/E)^3$, specifically dominating energies up to 500 keV. Therefore in the presence of high atomic number materials, energy can be transferred to the medium more effectively than water due to the photoelectrons ejected from the interaction of the photon with the inner electron shells[5] [6]. The de-excitation of the atom cannot be ignored when considering the spatial information of energy transfer. Fluorescence due to the differences in the incident photon energy and shell binding energy is a mode of de-excitation as well as Auger electrons. While Auger electrons have a shorter range and will most likely deposit their energy locally, fluorescence photons can travel larger distances based on their energy and therefore deposit energy and "dose" outside the region of interest. The result of this energy deposition by electrons is free radicals.

These free radicals, often ROS generated from water, are deleterious to the DNA repair process post-irradiation and are thought to be the main species produced by metallic nanomaterial[7]. ROS include hydroxyl radicals, superoxide radicals, and hydrogen peroxide[8]. Hydroxyl radicals (HO·) are responsible for up to 50-70% of DNA damage in clinical photon radiotherapy[9][10]. G-values (mol/J) are quantitative measurement of (HO·) overproduction in the presence of nanomaterials and can be convenient in making comparisons between studies with varying parameters. The production of (HO·) can be accomplished by three main pathways. The first pathway involves the incident radiation having a primary interaction with the nanoparticle. Electrons ejected from this interaction can interact with surrounding water and create (HO·) as a radiolysis product. The second pathway removes the role of the nanoparticle, having the incident radiation interact directly with water molecules and produce (HO·). The third pathway is a continuation of the second pathway. However, these radiolysis products then secondarily interact with the nanoparticle to produce further reactive species[9].

Multifunctional nanoparticles

The presence of foreign material in the body may have other advantages other than dosimetric radioenhancement, such as imaging. Computed tomography (CT), magnetic resonance imaging (MRI), positron-emission tomography (PET), single-photon emission tomography computed tomography (SPECT), and other imaging modalities are used in the radiotherapy process to visualize and delineate specific volumes. Contrast agents, such as gadolinium (Gd) or iodine (I) based, are often used in MRI and CT, respectively, to improve this delineation. The manipulation of the attenuation coefficients in associated tissues for CT and relaxation times in MRI allow for radiologists and technologists to more accurately read a patient's anatomy. The presence of high atomic number material is advantageous in CT imaging due to its high density as compared to typical anatomy, but primarily to induce differential photoelectric absorption. Fluorescence imaging also takes advantage of the luminescence properties of contrast agents and materials to visualize their accumulation in specific tissues during procedures like surgery. Rare-earth metals are common doping agents for these materials that allow for a bright fluorescence signal with a tunable plasmon resonance energy[11]. These rare earth metals include elements such as europium and terbium for emission of red and green luminescence respectively under ultra-violet (UV) and near-infrared (NIR) excitation[12].

II. Literature Review

Previous Studies

High atomic number material for dose enhancement has been investigated for the better part of a century. Gold nanoparticles have a historical role in this area of research due to their "relatively straightforward synthesis route, high stability in biocompatible solvents, low toxicity, and also good biodistribution and pharmacokinetics"[5]. Hainfeld at al. was the first group to demonstrate malignant tumor control in a pioneering in vivo study using high atomic number material when they injected 1.9nm gold nanoparticles into mice subjects with EMT-6 subcutaneous mammary tumors and irradiated in the kilovoltage range to a dose of 26 Gy[13]. Hainfeld et al. further observed CT image contrast and improved long term survival in mice with a highly malignant brain tumor irradiated with 100 kVp x-rays to a dose of 35 Gy using 11nm AuNPs[5][14]. Al Zaki et al. was another group that investigated CT image contrast and

radioenhancement in mice with HT-1080 human fibrosarcoma tumors using 1.9nm AuNPs inside polymeric micelles at a concentration of 650mg AuNPs/kg. A comparison was made to radiation treatment of mice without nanomaterial when treated with 6 Gy at 150 kVp. There they observed a 1.7 fold longer median survival time[5][15]. Other groups such as Miladi et al incorporated gadolinium chelates into their AuNP coatings to monitor biodistribution of the material using MRI and waiting until sufficient tumor uptake to treat 9L gliosarcoma brain tumor in mice via microbeam radiation therapy (MRT)[5][16]. An important distinction was made by McQuade et al. that exposed a fault in this theranostic approach to nanomaterial. The improved CT image contrast was achievable but at much higher concentrations of material injected than necessary to achieve radioenhancement, bringing about questions of biocompatibility and toxicity[5][17]. Therefore, MRI contrast material was investigated to achieve such image contrast at lower concentrations. These studies along with many others provided proof of concept; however, more relevant delivery parameters of radiation oncology such as megavoltage beams and increased dose rate needed to be investigated.

Many of the aforementioned studies can be observed as using lower energies and dose rates than what is used in modern radiation therapy. This was to take advantage of the high photoelectric absorption cross-section and generation of secondary electrons from nanomaterial using kV X-rays. However, as observed in many studies, megavoltage beams combined with nanomaterial has demonstrated radioenhancement despite the primary interaction mechanism being Compton scattering. This interaction produces recoil electrons that can be of low energy but this event also reduces the photon energy and will likely proceed to lose more energy through larger angle scatter. The recoil electrons could induce a cascade of scattering events that are localized to the nanomaterial[5]. This effect could also be enhanced by flattening filter-free (FFF) beams in a clinical setting which still contain keV level photons for photoelectric effect and electron contamination which could directly ionize the atoms in the nanomaterial. Different treatment modalities such as proton therapy and heavy ion therapy have also been investigated for use with nanomaterial to explore radioenhancement. Kim et al. is responsible for the two main in vivo studies investigating the effect of proton irradiation on 1.9 and 14nm AuNPs as well as 13-15nm superparamagnetic iron oxide nanoparticles. However, high concentrations of the particles injected are noted here but the group did not observe toxicity in the mice with CT26 mouse tumors treated with 41.7MeV spread-out Bragg peak (SOBP) beams[5][18][19]. Monte-

Carlo simulations have also been conducted, such as by Abolfazli et al. using MCNPX code, to study dose enhancement in the presence of megavoltage radiation and gold nanoparticles. The simulation was performed with a cobalt-60 source and 6MV (separately) parallel photon beam irradiating a cubic volume with 30 or 50nm gold spherical nanoparticles. Dose enhancement was found with the larger nanoparticles, decreasing with distance from the central axis. Additionally, 10- to 2000- fold increase in secondary electron production in the presence of AuNPs[20].

ROS measurement

While in vivo studies in cell lines can use survival fractions and other radiobiological metrics to quantify dose enhancement, measurement of ROS production in aqueous environments in vitro is a common and facile quantitative method to indicate enhancement. This also allows for the investigation of the production of ROS and specific ROS that are responsible for any observed radioenhancement. However, the short lifetime of HO· and the previous lack of sensitive assays have made the quantification technique of the specific free radical difficult. While the radical alone is not intensely useful for measurement, HO· will hydroxylate organic aromatic rings and these derivatives can be highly fluorescent[10]. Therefore this fluorescence is proportional to the amount of HO· set forth post-irradiation. These functional groups include benzoates, coumarins, and phenoxazines[10]. Coumarins are a category of photochemicals that have previously been used in multiple studies to detect HO· levels following radiation[21]. The coumarin HO· trapping assay is highly sensitive and is able to detect minimal concentrations of hydroxyl radicals, down to 30nM. This technique identified the dependence of 7-hydroxycoumarin (7OH) intensity on nanoparticle concentration, allowing the estimation of HO· production[9]. The fluorescent yield for 7-hydroxycoumarin-3-carboxylic acid via coumarin-3-carboxylic acid is estimated to be 4.7% per HO· in the absence of any added scavengers[10]. Radical scavengers can include acetone, acetonitrile, methyl alcohol, and dimethyl sulfoxide (DMSO), which prevent hydroxylation at the seventh ring position to create 7-hydroxycoumarin-3-carboxylic acid[10].

Enhancement Modes

There are three main accepted modes of radiation enhancement in the presence of nanomaterial: physical, chemical, and biological enhancement. Each category is subdivided into the specific mechanisms which define the process which were previously ambiguous to researchers. Guo provides a comprehensive review of these mechanisms and clarifies many definitions[22]. For this project, physical and chemical enhancement are the most pertinent modes.

Physical enhancement (PE) is defined as enhancement without the aid of chemical or biological processes, meaning energy transfer by non-catalytic reactions and without biological regulation[22]. The category can further be subdivided into Type 1 PE, Type 2 PE, and Type 3 PE based on the energy transfer and deposition from the external radiation to the tissue. Despite the separation of deposition mechanisms, there are often multiple types of enhancement present and contributing to radiation enhancement. Type 1 PE (T1PE) is characterized by uniform enhancement and energy deposition through electron interactions stemming from the nanoparticles throughout a sample volume. Due to T1PE and T2PE often being present simultaneously, specifically with larger nanoparticles, T1PE will dominate and account for the majority of enhancement. However, difficulties defining this mechanism are present. The presence of chemical enhancement and anti-enhancement can appear when T1PE is large. This also is dependent upon the probe being uniformly distributed over the entire volume.

Type 2 PE (T2PE) is seen near the surface of nanomaterial, instead of uniformly through the volume as in T1PE. The enhancement present is dependent upon the size and shape of the nanoparticles and is derived from particularly low energy electrons depositing their energy in close proximity to the nanomaterial surface. This enhancement is also difficult to characterize due to the placement of the probe. If uniformly distributed, the probe will most likely see T1PE but if placed near the surface of the nanomaterial, increased T2PE will be detected.

Type 3 PE (T3PE) can be further bifurcated into two specific types: T3PE(1) and T3PE(2). T3PE(1) is the most common between the two and results in the emission of UV-VIS photons from the X-rays being absorbed in the nanomaterial and the subsequent electrons transfer energy to the semiconductor/rare earth material. T3PE(2) results from the X-ray energy being absorbed by the medium and subsequent electrons originating from outside the material excite the semiconductor/rare earth and produce the photons. Materials of a low atomic number are more

likely to cause T3PE(2) due to electron-hole pairs being created in the medium because the nanomaterial has a lower affinity to absorb the x-ray energy.

Discrepancies in predictive models (Monte-Carlo based) for dose enhancement and experimental results indicated that physical enhancement could not be solely responsible for the observed enhancements[23]. Chemical and biological enhancement mechanisms have also been proposed. Chemical enhancement examines the role of the nanomaterial in the chemical reactions that occur in the environment post-irradiation. Well-characterized materials that have been previously investigated for the composition of nanoparticles include silver, gold, platinum, silica, and more[24]. The selection of these materials included a key characteristic of being unreactive and chemically inert. However, this is no longer a valid assumption due to unaccounted for enhancement and now must be reviewed as a catalyst. In the review by Guo, chemical enhancement is segmented into type 1 (T1CE) and type 2 chemical enhancement (T2CE). The difference between the two relies primarily on whether there is an increased production of ROS present. T1CE reports no significant increase in ROS but rather enhancement due to the catalytically active surface of the nanoparticle. This can also include catalysis of DNA strand break reactions and polymerization[23]. T2CE does report increased ROS production but attributes this as a catalytic increase due to the nanomaterial chemically reacting with the environment. Also identified as a dynamic chemical enhancement, it requires the activation of the nanomaterials by superoxides generated from radiation while PE requires increased absorption by the nanomaterial to produce the radical groups under irradiation[23].

Biological enhancement is the result of electrons from the surface of nanomaterial interacting with an aqueous environment to produce ROS whose DNA damage effects have been previously mentioned. However, biological enhancement is seen with or without the use of ionizing radiation and solely in the presence of nanomaterial to send cells into oxidative stress and damage primary targets such as the mitochondria and induce cytotoxicity. Evidence of cell cycle effects distributing cells into radiosensitive phases such as G1/M or disrupting cell cycle checkpoints in the presence of GNP and other materials have been reported. The bystander and abscopal effects have also been considered due to the influence nanomaterial can have on cell to cell communication and influence production of intercellular signals such as ROS and cytokines. This could, therefore, affect cells that have not been directly exposed to radiation and warrant a response outside the affected region[25].

Enhancement Units

To quantify enhancement, metrics have been created and used in the literature to allow quantitative analysis of results. Dose enhancement can be quantified by dose enhancements units, DEUs[22][23]. An important distinction to note is whether the DEUs are relative or absolute values. DEU is calculated by using the ratio of measured signal with nanomaterial to that without nanomaterial. It is vital to consider the ROS production of the irradiated material, coumarin-3-carboxylic acid, without nanomaterial present in order to establish enhancement when present. This calculation would be a relative value, while this value minus one is an absolute DEU[22]. For this project, the fluorescence signal measured of the 7-hydroxycoumarin-3-carboxylic acid (7-OH-CCA) will be the benchmark of enhancement. These calculations are demonstrated in Equations 1 and 2. Specific to radiation oncology and therapeutic applications, dose enhancement ratios (DER) are also quoted in the literature.

$$(1) \qquad Relative\ DEU = \frac{7{-}OH{-}CCA\ with\ NP}{7{-}OH{-}CCA\ without\ NP}$$

$$(2) \qquad Absolute\ DEU = \frac{7{-}OH{-}CCA\ with\ NP}{7{-}OH{-}CCA\ without\ NP} - 1$$

Another metric has been proposed recently in addition to DER and bridge the gap of discrepancies between radiobiological results and theoretical predictions. Linear energy transport enhancement ratio (LETER) has been addressed by Gadoue and Toomeh for the first time via the radiation transport code SCEPTRE[26]. The equation for LETER can be seen in Equation 3. The motivation for introducing investigation into linear energy transfer (LET) stemmed from the metric's association with biological effects. As more energy is lost per unit distance of the secondary charged particles track, more and densely packed ionization events can occur along the path and therefore can induce significant biological damage in the immediate spatial area. Previous studies have demonstrated increases in LET of secondary electrons near GNPs as well as at the nanomaterial and soft tissue interfaces. This new metric could be more effective in associating radiobiological consequences and predicting outcomes based on the parameters selected. During Gadoue and Toomeh's simulations, they were able to demonstrate a lower

LETER than DER at 120kVp with both 50nm and 100nm GNP. Using 100nm GNP, however, LETER decreased even more so than with the 50nm simulation, most likely due to self-absorption of low energy secondary electrons. At 6MV energy, they were able to demonstrate higher LETER values than DER which increased with larger GNPs. While more investigation into using this metric is needed, this theory could account for previous discrepancies in experimental results.

$$(3) \qquad LETER = \frac{Average\ LET\ due\ to\ secondary\ particles\ in\ the\ presence\ of\ GNP}{Average\ LET\ due\ to\ secondary\ particles\ without\ GNP}$$

III. Objectives

To synthesize and characterize nanoparticles composed of high atomic number elements and semiconductor material in a core/shell structure for the potential to be used as sensitizers for radiotherapy as well as in luminescence imaging platforms. Additionally, we sought to quantify their role in free radical production after exposure to ionizing radiation through chemical routes to investigate their role in radioenhancement.

IV. Methods

The synthesis of the core/shell nanoparticle required a variety of protocols and characterization at progressive stages of completion. The gold cores were synthesized first and then characterized to allow for adjustment and an analysis of size control. Once the core samples were prepared, they were then characterized by a variety of techniques as described later in this section. After the completion of the gold cores (AuNPs), the spherical nanoparticles of both diameters were used separately to create the europium-doped gadolinium vanadate flower-like nanoparticles (Au/$GdVO_4$:Eu NPs). These final product nanoparticles were then characterized and compared to the synthesis protocol for analysis. After confirmation of the composition and geometry of both AuNPs and Au/$GdVO_4$:Eu NPs, irradiation protocols were followed as well as measurement techniques. Each of these steps will be described in the following section.

Gold Nanoparticle Core Synthesis

Two diameters were selected for the spherical gold nanoparticles that would serve as the core for the flower-like nanoparticle. Synthesis protocols for diameters of 12 nm and 25 nm were carefully chosen to explore the size dependence of the radiation enhancement on the amount of gold present in the sample, as well as a different basis for building the luminescent shells. Turkevich et al. established the underlying protocol for the synthesis of colloidal gold and the method for size control via citrate stabilization [27]. While the nucleation and growth processes are constant, different heating times, concentrations, and chemical amounts are varied to control the diameters of the spherical nanoparticles. Sodium citrate and gold chloride are the chemical basis for both these synthesis methods. It should be noted here that each sample underwent cleaning cycles before imaging and irradiation. This cleaning technique involves centrifuging the samples to induce precipitation of the particles and removing the supernatant. The exact volume extracted was then replaced with water. This is a mandatory step in the preparation process due to the influence the chemicals, primarily sodium citrate, could have on the characterization techniques as well as its potential to act as a radical scavenger therein reducing the presence of hydroxyl radicals and reducing fluorescence measurement[28].

12nm Gold Nanoparticle Core Synthesis Method

50 mL of 1mM hydrogen tetrachloroaurate was added to a 100 mL volumetric flask with stopper. The solution was brought to 80° C on a hot plate with vigorous magnetic stirring. Once at 80° C 0.2 mL of 1 M trisodium citrate was added to the solution. The solution was then maintained at 80° C with stirring for 25 minutes with temperature checks every 3-5 minutes with a thermometer. The red wine color solution was cooled to room temperature and stored with limited light exposure [27]. The concentration of gold within each sample of the solution was 0.23 g/L.

25nm Gold Nanoparticle Core Synthesis Method

135 **μ**L of 0.1M trisodium citrate was added to 50 mL of ultrapure water in a 100 mL volumetric flask with stopper. The solution was brought to 80°C on a hot plate with vigorous magnetic stirring. Once at 80°C, 250 **μ**L of 50mM hydrogen tetrachloroaurate was added to the solution.

The solution was then maintained at 80°C with stirring for 25 minutes with temperature checks every 3-5 minutes with a thermometer. The solution was cooled to room temperature and stored with limited light exposure [11]. The concentration of gold within each sample of the solution was 0.057 g/L. In order to maintain a consistent concentration of gold between the two sizes of gold nanoparticles in the measured samples, these larger particles were centrifuged (10000 rpm for 10 minutes) and underwent volume reduction (50.385 mL to 12.551 mL) to raise the concentration to that of the smaller gold nanoparticles, 0.23 g/L.

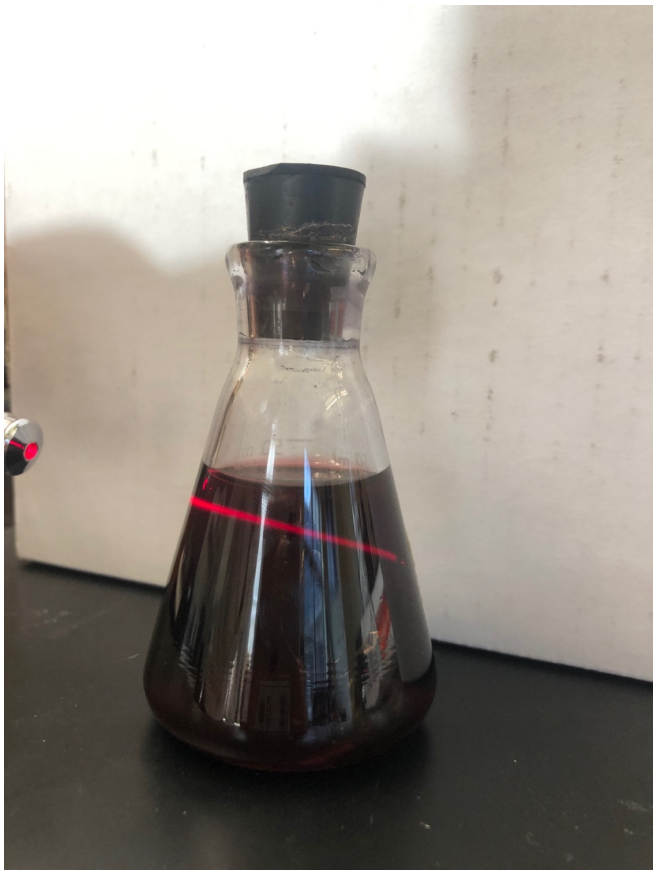

Figure 1.) Gold nanoparticles in solution after synthesis

Au/$GdVO_4$:Eu Core/Shell Nanoparticle Synthesis

A facile protocol was selected using sodium citrate as a stabilizer for the gold nanoparticle cores, but also as a linker/chelating agent, stabilizer, and soft template for the shell[11]. The citrate's role in the process allows for full nucleation onto the core and growth of the heterogeneous structure.

0.6 mL of 0.1 M trisodium citrate was added to 10 mL of the gold nanoparticle solution, as prepared above, under magnetic stirring. 200 **µ**L of 0.01 M $Gd(NO_3)_3$ aqueous solution containing 5% $Eu(NO_3)_3$ and 100 **µ**L of 0.1 M Na_3VO_4 was injected into the former solution. The solution was then transferred to the 20 mL Teflon bottle for placement inside the stainless steel pressure vessel. The solution was then sealed and maintained in the oven at 200°C for two hours. The vessel was then left to cool to room temperature until centrifugation. The solution was then transferred to a centrifugation vial and centrifuged at 8000 rpm for 8 minutes (Eppendorf Centrifuge 5804 R). The nanoparticle solution was then cleaned by removing supernatant containing surfactant residues and replacing it with purified water [11]. A schematic of this process can be seen in Figure 2. These nanoparticles in solution were also seen to have a bright red emission under UV irradiation as can be seen in Figure 3.

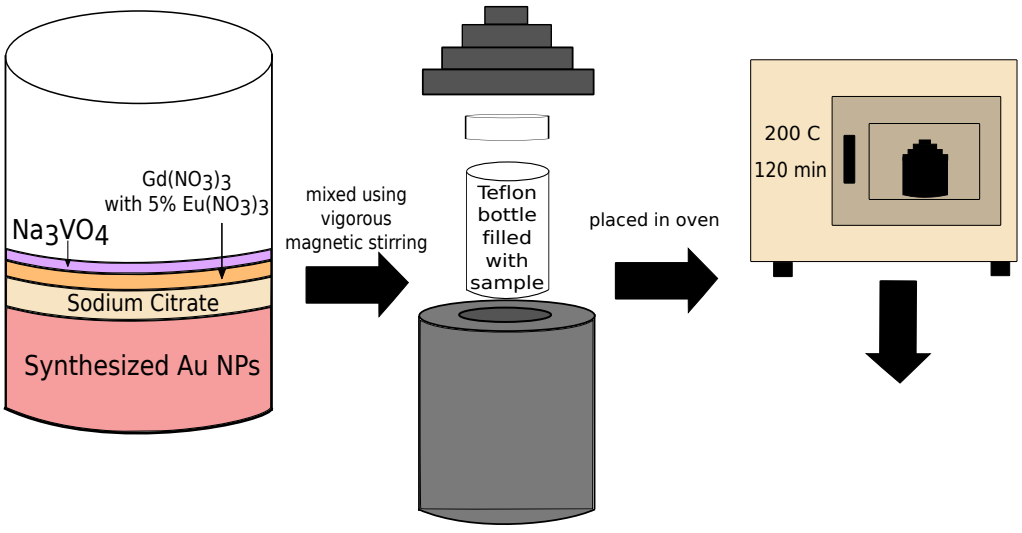

Figure 2.) Schematic of Au/$GdVO_4$:Eu synthesis via extended heating in a pressurized vessel.

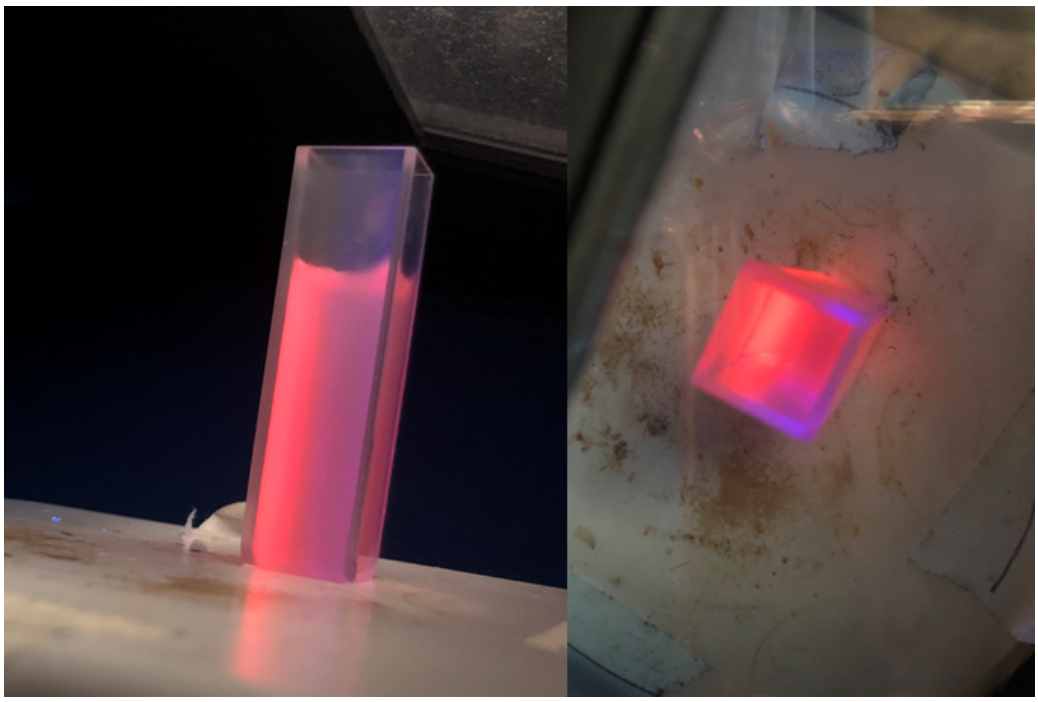

Figure 3.) Au/$GdVO_4$:Eu bright red luminescence property under UV irradiation.

Characterization Techniques

Two techniques were employed to characterize both the spherical cores and flower-like nanoparticles. These techniques were scanning transmission electron microscopy (STEM) and UV-VIS spectroscopy.

i. Scanning Electron Microscopy (SEM)

Images of the gold cores and synthesized core/shells were obtained by using STEM. This was a visual confirmation of the geometrical configuration of both the spherical cores and flower-like structural shells. Software, ImageJ, was also utilized to also verify the size of the synthesized particles and obtain particle size distributions data that is listed in the Results section of this work. This software uses the SEM images to set the scale and allow for accurate measurements of each individual particle diameter. Approximately 500 nanoparticle measurements were used to create the distributions.

ii. Ultraviolet-Visible Spectroscopy (UV-VIS)

UV-VIS spectroscopy with a Thermo Scientific Genesys 10S UV-Vis Spectrophotometer (Waltham, MA) was performed on the core and core/shell nanomaterials to identify the absorption peaks and analyze the constituent material. This was performed firstly on the gold nanospheres alone and then when the shells were created deposited to examine the changes in optical properties.

Quantification Technique

i. Coumarin-3-carboxylic acid

Alfa Aesar (Portland, OR) coumarin-3-carboxylic acid 98% was purchased and utilized for this experimental protocol. Solutions at concentrations of 1mM and 2mM, were selected to be combined with nanoparticle suspension in order to compare the differences in hydroxyl radical production when the concentration of nanoparticles present varied. Therein, the concentration of the coumarin-3-carboxylic acid would be kept constant at 0.5mM in all irradiation experiments and not influence the hydroxyl radical production. A separate solution at a concentration of 0.5mM was made and irradiated without nanoparticles to establish a baseline measurement for enhancement.

ii. 7-hydroxycoumarin-3-carboxylic acid

7-hydroxycoumarin-3-carboxylic acid was selected to be the fluorescent derivative of interest in irradiated coumarin-3-carboxylic acid that would be the focus of this quantification. According to manufacturing information provided as well as findings by Nafradi et al, the excitation wavelength was determined to be 342nm and the maximum emission wavelength was 447nm[21]. Due to the light sensitivity of the material and dependency on environmental conditions, the chemical was stored in the freezer when not in use. TCI AMERICA (Boston, MA) 7-hydroxycoumarin-3-carboxylic Acid 98% was utilized for this calibration curve. The calibration curve of various prepared concentrations of 7-hydroxycoumarin-3-carboxylic acid allow an association to be made between the amount of the fluorescent derivative present (associated with the amount of HO• present) and the

measured fluorescence intensity. A sample of 7-hydroxycoumarin-3-carboxylic acid under UV irradiation can be seen in Figure 4.

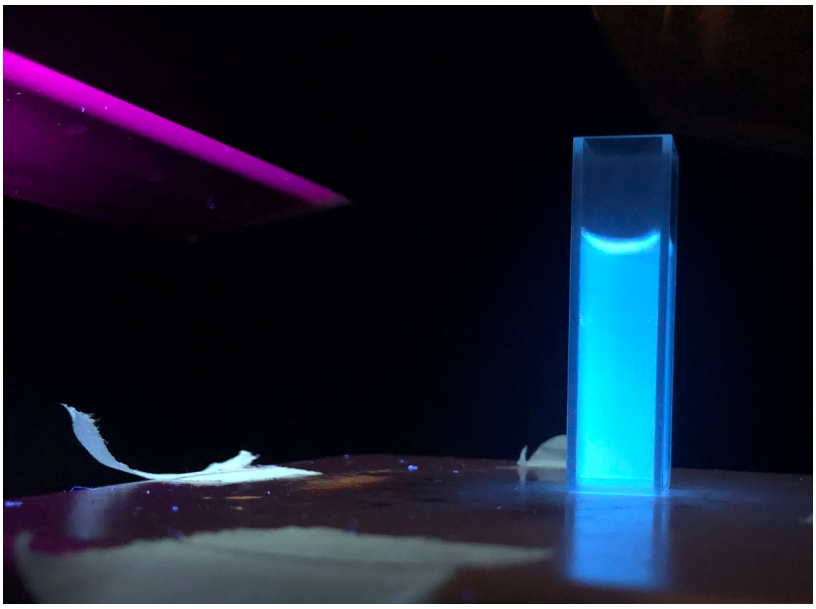

Figure 4.) Sample of 7-hydroxycoumarin-3-carboxylic acid fluorescence.

iii. Fluorescence Detection

An Ocean Optics Flame VIS-NIR Fluorescence Miniature Spectrometer was used as the apparatus to measure the fluorescence intensities of the samples. A deuterium lamp was the light source used for this measurement. Associated accessories to the experimental setup such as two Ocean Optics fiber optic cables, four-sided quartz cuvette with 1cm path length (ThorLabs, Newton, NJ), and cuvette housing with covering (to prevent detector saturation) was utilized. This experimental setup is pictured below in Figure 5. In addition to the consistent setup of the apparatus, the associated Ocean Optics software Ocean View 1.67 was utilized for analysis. The analysis procedure was kept consistent across every fluorescence measurement to increase the sensitivity of the signal and obtain a desirable fluorescence spectrum. The protocol selected was 10 scans averaged together each lasting 5 seconds with a boxcar width of 10 to appropriately smooth the spectrum and average adjacent points without reducing the spectral resolution significantly. This resulted in the measurement cycle lasting 50 seconds each. A background scan was recorded before each measurement session with a sample in the cuvette holder to be able to remove ambient signals from the

measurements. If the recorded spectrum was found to be noisy or with unexpected peaks, an additional background scan was recorded to remove the influence of signals such as detector saturation or light leakage. It should be noted that there was a consistent signal found to be at 450nm in all data recorded with the spectrometer. It was determined to be a defect within the equipment and this was cautiously considered in spectral analysis.

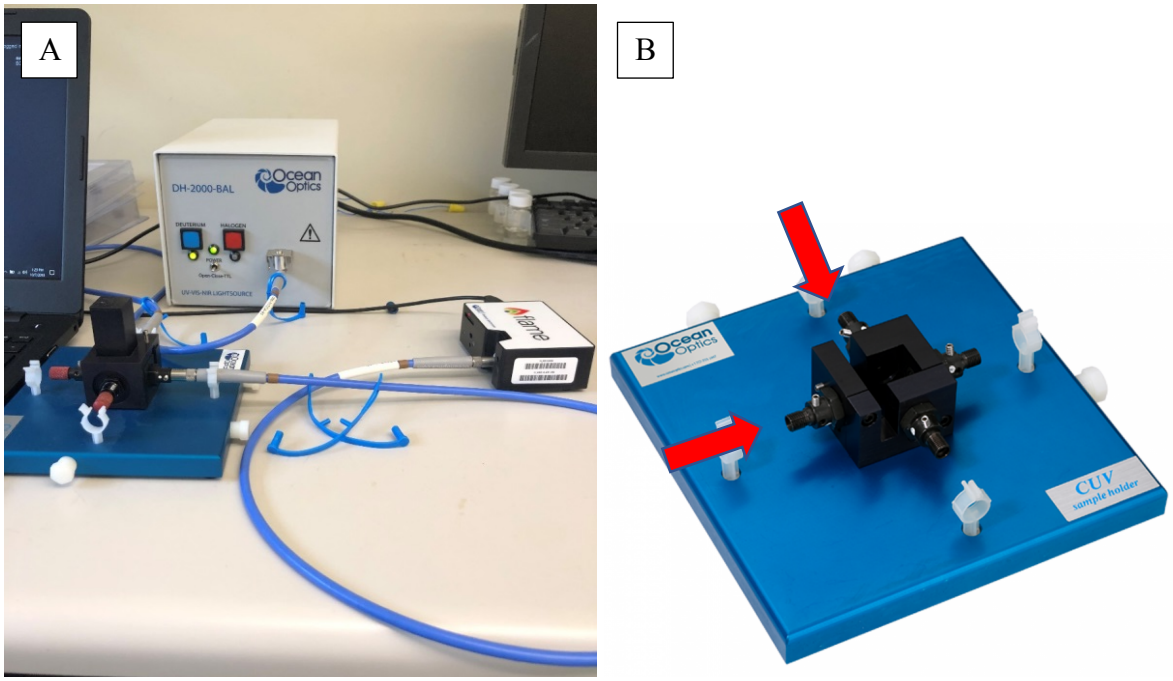

Figure 5: A) Experimental setup for fluorescence measurement. B)* 90° placement of fibre optic cable for measurement. *Adapted from Ocean Optics.

iv. 7-Hydroxycoumarin-3-carboxylic acid calibration curve

To establish the fluorescence intensity associated with the measurement of irradiated coumarin-3-carboxylic acid and therefore 7-hydroxycoumarin-3-carboxylic acid (the fluorescent derivative), varying concentrations of 7-hydroxycoumarin-3-carboxylic acid were prepared and measured. Various concentrations ranging from 0.1-4 µM were calculated, prepared, and measured with the previously mentioned apparatus. These concentrations were selected for two reasons. One, they were reasonable predictions of the concentration of 7-hydroxycoumarin-3-carboxylic acid after irradiation. Second, to establish a well-defined

calibration curve over a wide range of concentrations and analyze the accuracy of the counts obtained from the detector at each concentration. Serial dilution was performed in order to obtain the various concentrations while economically preserving the material. Each concentration was prepared three times to establish reproducibility and obtain a standard deviation for the counts of each sample. The three replicates were averaged and used for the calibration curve values at the maximum emission wavelength (~447nm)[4]. Note, these concentrations were prepared with ethyl alcohol 95% (Fisher Science Education) for better solubility and uniform distribution of the solid chemical. Newton and Milligan previously investigated the role of radical scavengers on the detection of fluorescent product yields to confirm that the hydroxyl radical is responsible for the formation of the fluorescent derivatives after irradiation[10].

Sample Preparation for Irradiation

A Precision X-Ray X-Rad 225 XL irradiator was utilized to deliver varying doses to the prepared samples using ionizing x-rays. No collimation or filtering was used when delivering the treatment. Doses of 50, 100, 150, and 200 Gray were delivered to the samples to establish a dose dependence and compare to previous literature results. The irradiation protocol was set for 225 keV, 13.3 mAs, and an SSD of 12cm. The dose rate of 12,762 cGy/min as provided by the manufacturer made for irradiation times of 24, 48, 72, and 96 seconds for doses of 50, 100, 150, and 200 Gy respectively. This device can be seen in Figure 6.

Figure 6.) The X-RAD 225 XL irradiator used for the experimental procedures.

Irradiation Protocol

In order to investigate the radiation enhancement in aqueous environment in the presence of the manufactured nanoparticles and establish them as radiosensitizers, the irradiation protocol was performed on multiple materials. These materials included the following:

1. 0.5mM 3-coumarin-carboxylic acid without nanoparticles
2. 1.5mL of 1mM 3-coumarin-carboxylic acid with 1.5mL of 25nm gold cores
3. 0.75mL of 2mM 3-coumarin-carboxylic acid with 2.25 mL of 25nm gold cores
4. 1.5mL of 1mM 3-coumarin-carboxylic acid with 1.5mL of 12 nm Au/$GdVO_4$:Eu core/shell nanoparticles
5. 1.5mL of 1mM 3-coumarin-carboxylic acid with 1.5mL of 25 nm Au/$GdVO_4$:Eu core/shell nanoparticles
6. 0.75mL of 2mM 3-coumarin-carboxylic acid with 2.25mL of 12 nm Au/$GdVO_4$:Eu core/shell nanoparticles

7. 0.75mL of 2mM 3-coumarin-carboxylic acid with 2.25mL of 25 nm Au/$GdVO_4$:Eu core/shell nanoparticles

i. Gold nanoparticle irradiation

Irradiation of the gold cores was performed to establish the role of the high atomic material within the sample if radiosensitization was to be induced. Additionally, this data would be compared to the irradiation of the full core/shell nanoparticle synthesized to investigate the performance of the shell, when introducing new elements and geometry, in the presence of ionizing radiation. An important step that will be seen in both the core and core/shell fluorescence measurement will be the removal of the nanomaterial prior to the fluorescence spectra being recorded. It has been observed that increased incubation times of the nanomaterial with the oxidized coumarin results in decreased fluorescence intensities, with the signal decrease being exacerbated at higher doses[9]. This supports protocols with short irradiation times and swift removal of supernatant for measurement for more accurate data collection.

1.5mL of 25nm spherical gold nanoparticles, at the concentration provided in the manufacturing procedure, was injected with 1.5mL of 1mM coumarin-3-carboxlic acid. This would produce a AuNP concentration of 0.55mM. The sample was prepared in a small acrylic container to be placed in the irradiator. This same container was used consistently for all irradiations, with appropriate cleaning in between. The presence of 7-hydroxycoumarin-3-carboxylic-acid was then measured using the fluorescence apparatus as described above for each dose administered. To avoid quenching of the fluorescence signal as a function of contact time between the nanoparticles and hydroxylated coumarin, the sample was centrifuged at 10,000 rpm for 3 minutes with intermediate acceleration and deceleration settings[9]. The supernatant liquid removed was then placed in the fluorescence spectrometer, therefore removing the nanoparticles from the solution.

Then, 2.25mL of spherical gold nanoparticles, of either size, was injected with 0.75mL 2mM coumarin-3-carboxylic acid. This would produce a AuNP concentration of 0.825mM. The same irradiation protocol and measurement technique was used to measure these samples. This was done to investigate the production of 7-hydroxycoumarin-3-carboxylic acid in the presence of different amounts of gold and with different concentrations of coumarin-3-carboxylic acid.

It should be noted that due to the nature of the 12 nm AuNPs, cleaning was not readily achievable via centrifugation. Extensive amounts of centrifugal force and time would be required to clean these very small particles. The 12nm AuNPs were not irradiated without shells due to the presence of sodium citrate and observed signal quenching. However, they were still utilized in the shell synthesis.

ii. Core/shell nanoparticle irradiation

A very similar irradiation protocol to the gold core irradiation was followed for the core/shell nanoparticles. Two amounts of the nanoparticle solution were selected to be irradiated to investigate hydroxyl radical production in the presence of various amounts of nanomaterial. However, once again the coumarin-3-carboxylic-acid would be maintained at 0.5mM using various amounts of nanomaterial solution with 1mM and 2mM prepared coumarin-3-carboxylic acid. The original concentration of nanoparticle solution was calculated to be 0.184 mM of $GdVO_4$. Once again 1.5mL NPs were combined with 1mM 3-CCA for irradiation. Centrifugation of 10,000rpm for 2 minutes at maximum acceleration and deceleration settings was utilized to prevent signal quenching. When combined with 3-CCA, the concentrations of $GdVO_4$ in solution were calculated to be 0.092 mM and 0.138 mM.

V. Results

Morphological characterization of the 12nm AuNPs

The 12nm AuNP cores were successfully synthesized via the stated method. However, as can be seen in Figure 7 A, the first trial of synthesis, performed at a temperature of 90°C for 15 minutes, resulted in larger particles and variability in size than anticipated. According to the literature and the original work of Turkevich et al. ,[27], the synthesis temperature and heating time plays an important role in the final characteristics of the product. Therefore, the synthesis procedure was optimized after consulting by reducing the synthesis temperature to 80°C and increasing the time to 25 minutes. As seen in Figure 7 B, C, D, the resulting particles in the following trials were approximately 12nm in diameter with a reasonable standard deviation

~10%. These size distributions were obtained with the software ImageJ measuring the individual particles in the STEM images of each sample, with an average of 500 particles measured per distribution.

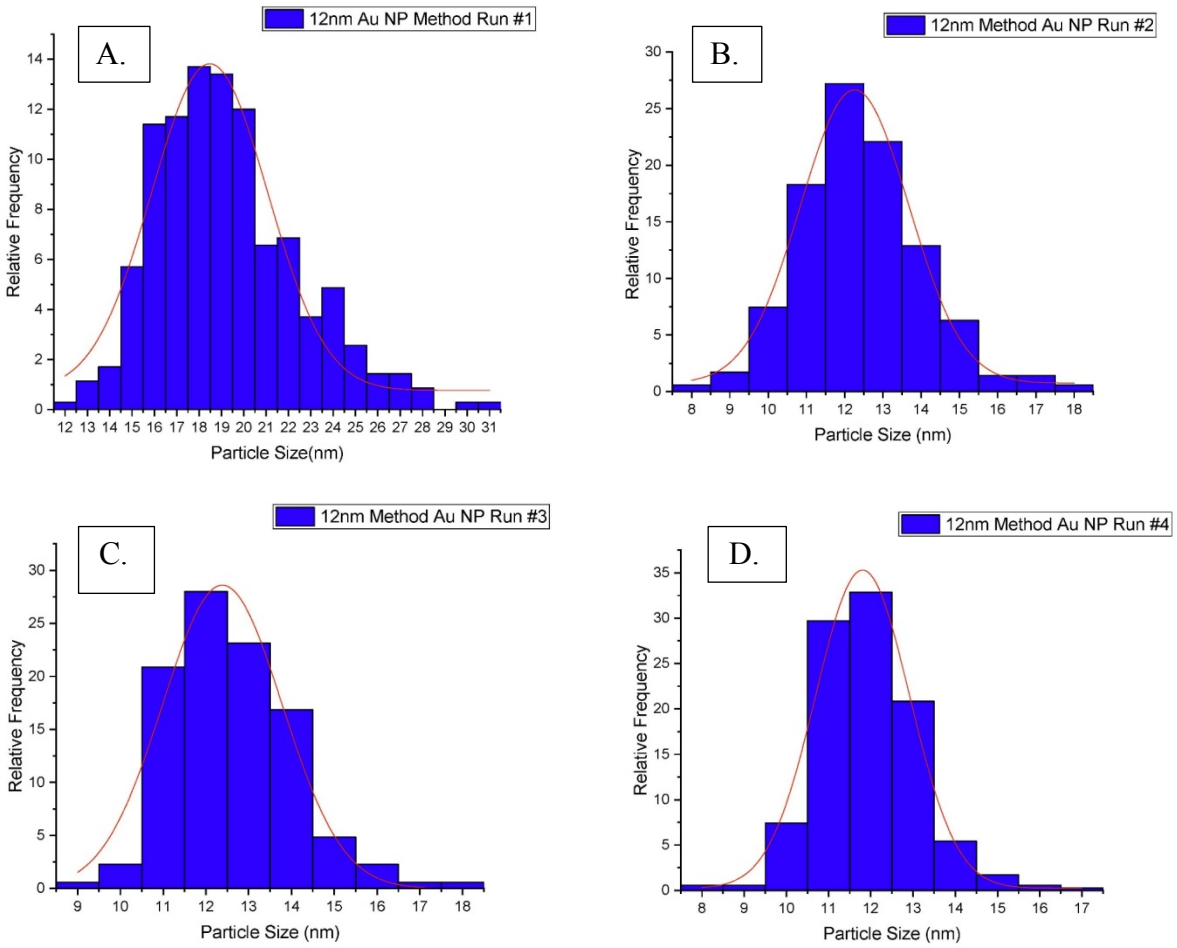

Figure 7.) Particle size distribution of synthesized 12nm gold cores. A) Run #1 19.2 ± 3.16 nm* B) Run #2 12.4 ±1.58 nm C) Run #3 12.7 ± 1.41 nm D) Run #4 11.9 ± 1.22 nm. *Change in protocol after Figure 7A to achieve improved size control in Figure 7B-D.

Morphological characterization of the 25nm AuNPs

The synthesis protocol for the 25nm AuNPs was also considered successful and reproducible. Figure 8 shows the size distribution of the synthesized particles once again roughly measuring 25nm with a ~10% standard deviation.

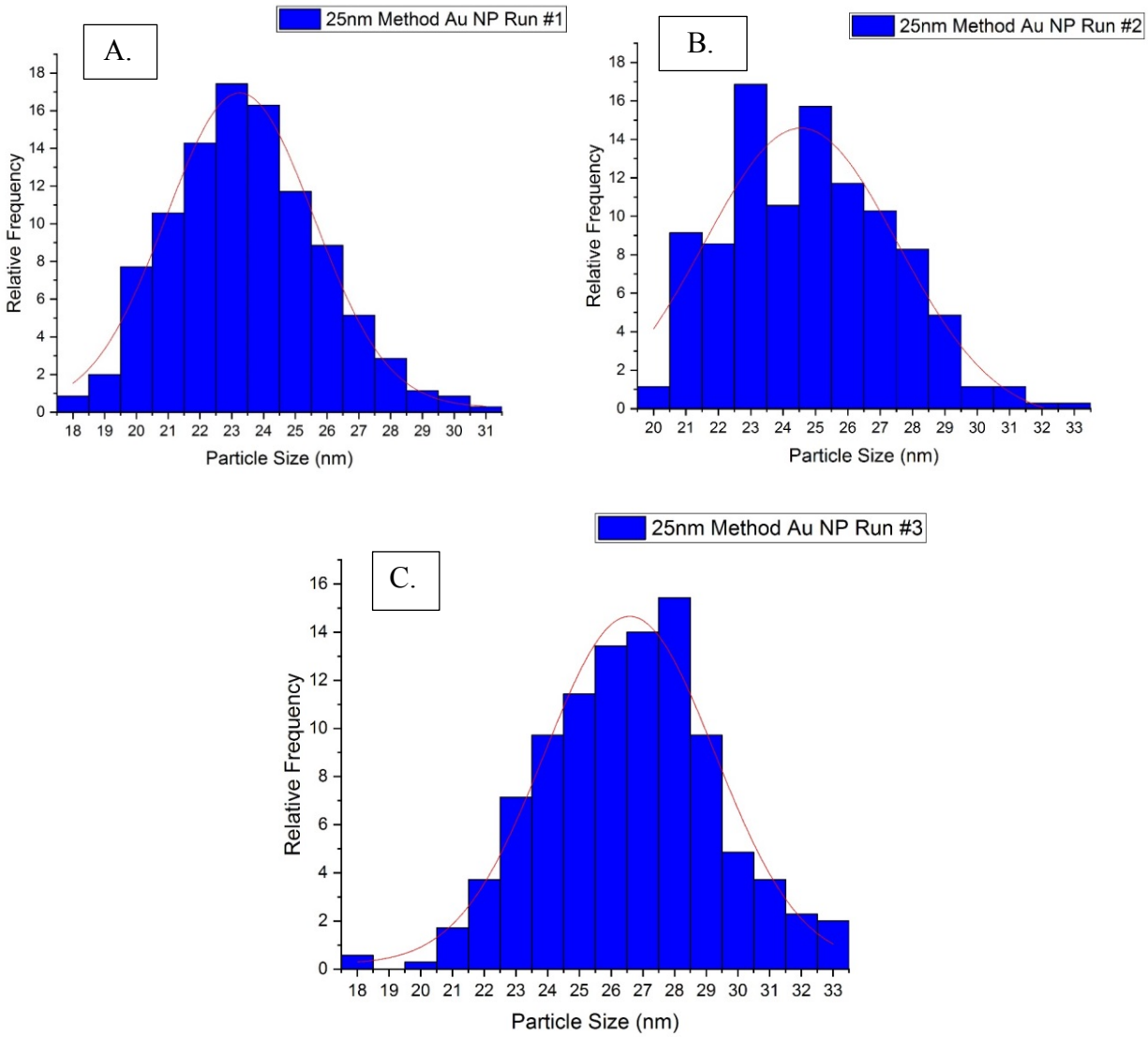

Figure 8.) Particle size distribution of synthesized 25nm gold cores. A) Run #1 23.4 ± 2.34 nm B) Run #2 24.8 ±2.48 nm C) Run #3 26.5 ± 2.78 nm

STEM

STEM images are displayed in Figure 9. A multitude of these images were used to obtain the size distributions above. This also allowed for a visual confirmation of spherical and core/shell geometries. The Au/$GdVO_4$:Eu as seen in Figure 9C visualizes the gold spherical core seen in the center of the associated shell and confirms the foundation of the shell being centered around the Au NP.

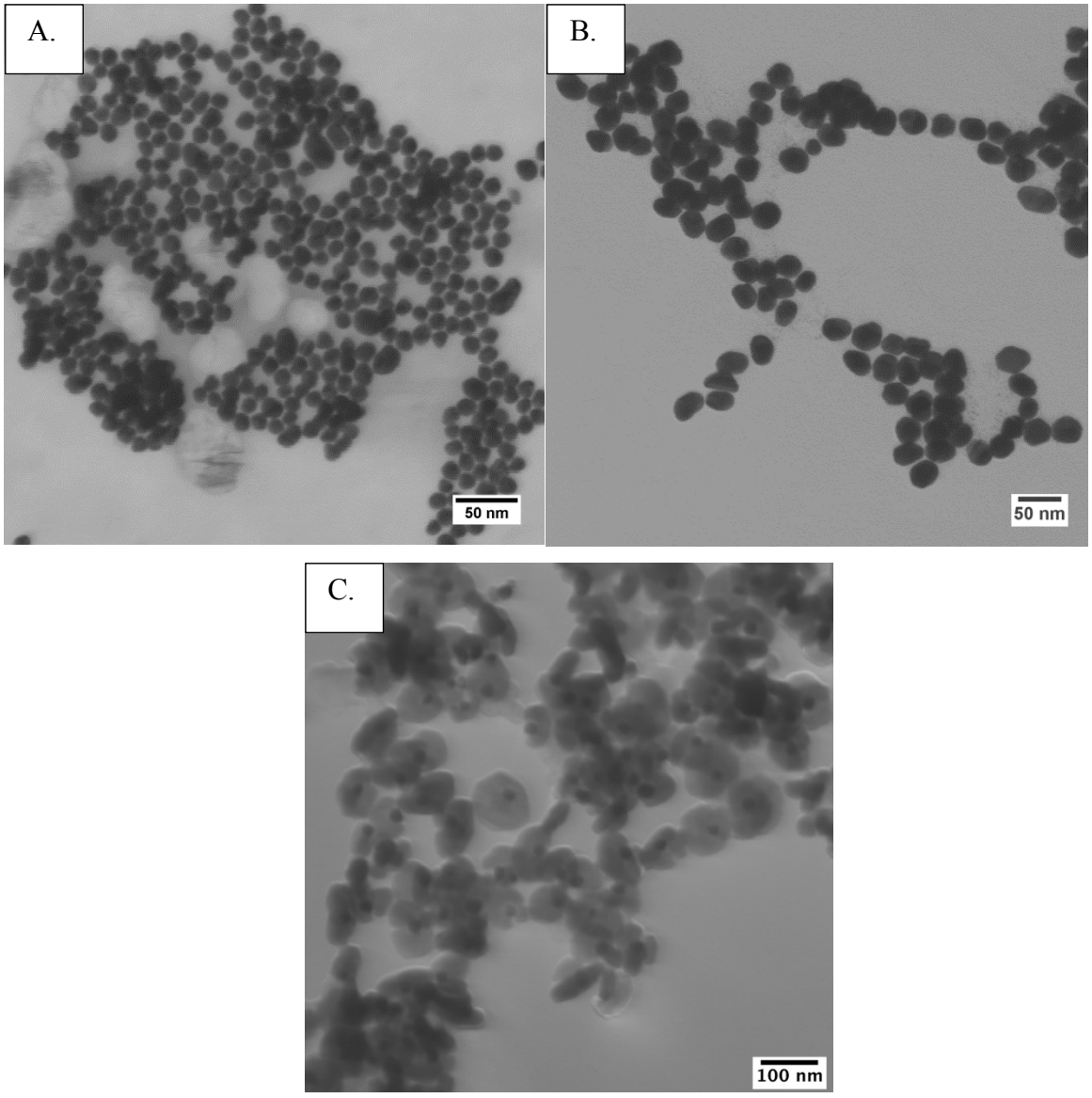

Figure 9.) STEM images obtained with Ultra High-Resolution Analytical FE-SEM SU-70 of A) 12nm gold cores B) 25nm cores C) Au/$GdVO_4$:Eu NPs

UV-VIS

Two main peaks were identified for each of the synthesized materials. A peak around ~274nm is present due to the sodium orthovanadate within the sample. The second peak is surface plasmon resonance peak observed in gold nanoparticles, and it is dependent on their sizes. The peaks seen in Figure 10A at 520nm and Figure 10B at 527nm for 12nm and 25nm gold cores respectively are within the correct range for absorption peaks for those sizes. The other peak seen is the result of absorption spectra of the Au/$GdVO_4$:Eu nanoparticles. According to the synthesis protocol, red-shifting of this peak from 542nm to 562nm was observed at 0.5 hours of heating versus 12 hours of heating respectively[11]. However, our results reveal that instead of red-shifting, peak broadening can be observed. Due to this, a heating time of two hours was selected due to evidence that the shell was present and fully formed with sufficient thickness by that point.

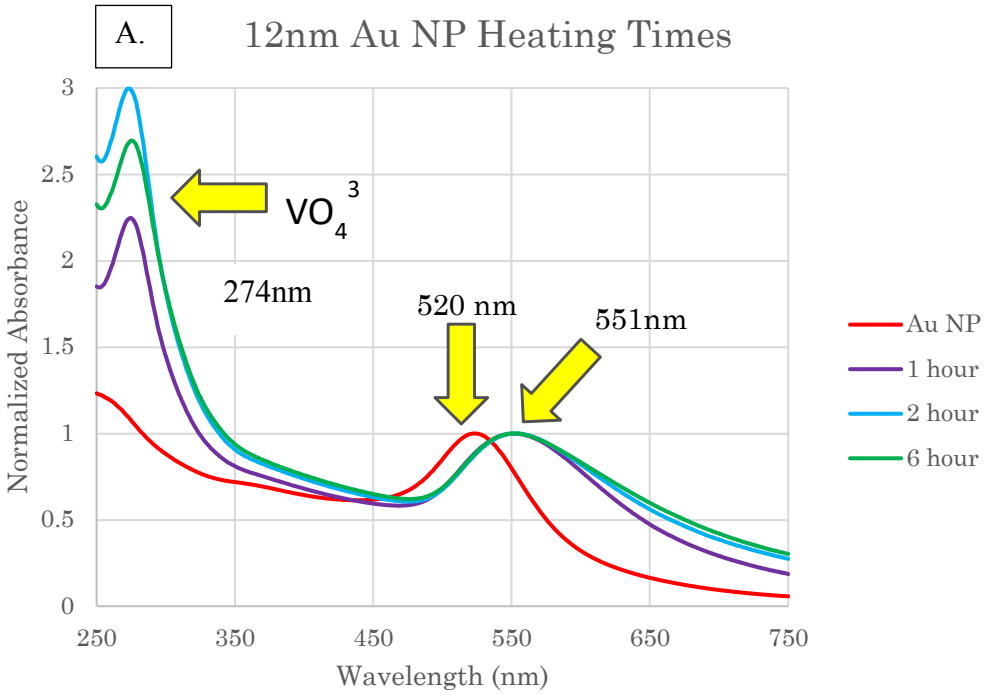

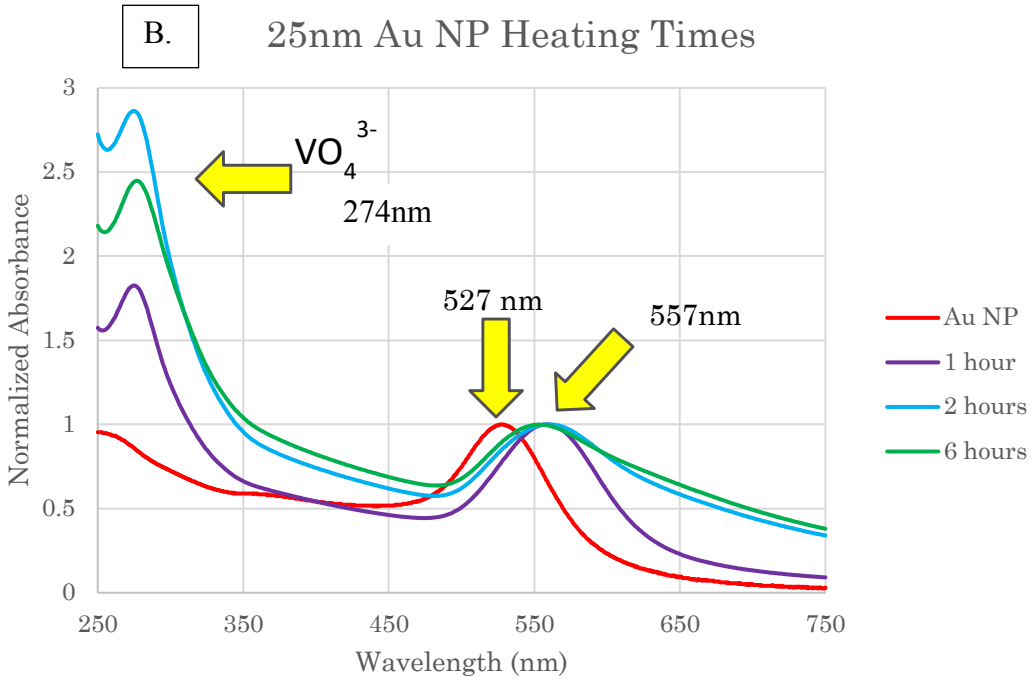

Figure 10.) Absorption spectra of Au/$GdVO_4$:Eu nanoparticles with various sizes of Au cores and the effect of heating times A.) 12nm cores B.) 25nm cores

7-Hydroxycoumarin-3-Carboxylic Acid (7-OH-CCA) Calibration Curve

The curve seen in Figure 11 corresponds to the calibration curve for different concentrations of 7-OH-CCA and their associated fluorescence intensities at ~447nm. Three solutions of each concentration ranging from 0.1-4μM were prepared and placed in the quartz cuvette for fluorescence measurement. The same quartz cuvettes with 1 cm path length would be used to measure the irradiated samples. As expected, a strong linear correlation is seen between the concentration and the respective fluorescence intensity, resulting in a coefficient of determination of 0.9991 of the linear fitting. The obtained equation of y=469x+13.2 would allow for 7-OH-CCA estimations to be made in irradiated samples and therefore comparatively measure the amount of OH radicals present.

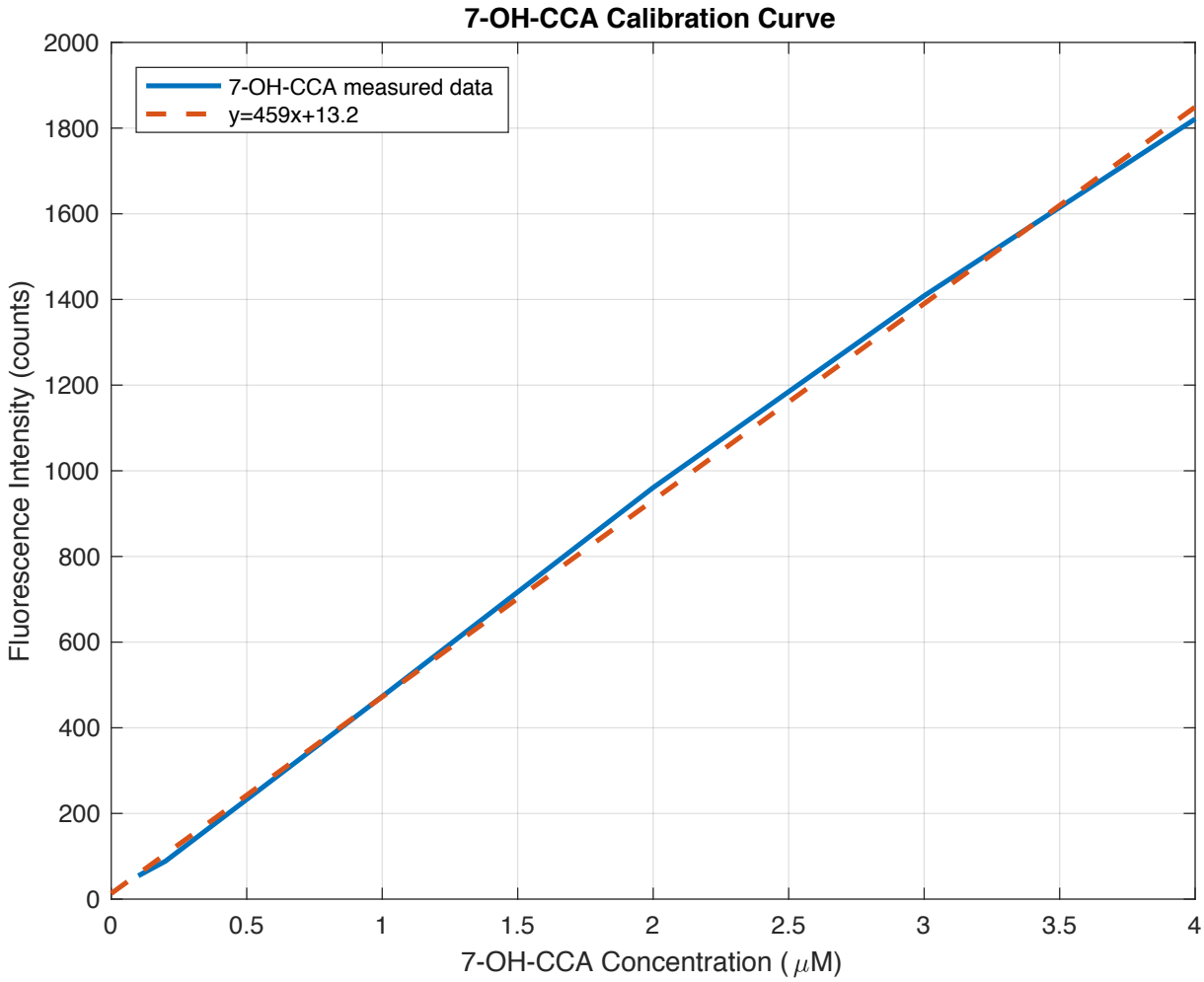

Figure 11.) 7-Hydroxycoumarin-3-carboxylic acid calibration curve

0.5mM Coumarin-3-Carboxylic Acid (3-CCA) Irradiated without nanomaterial

A concentration of 0.5mM 3-CCA was irradiated with no nanomaterial in the sample to establish a comparison when no nanomaterial was present. This would be the concentration of 3-CCA in all samples, including those with nanomaterial due to the dilution of the solution from the nanomaterial being dispersed in water. Fluorescence intensities were measured at approximately 125, 175, 250, 300, and 350 counts for 0, 50, 100, 150, and 200 Gy respectively. A linear fit of the data revealed a coefficient of determination of 0.9935 and fitted equation of y=1.16x+127, maintaining a linear relationship without nanomaterial present. For the

representation of the data in Figure 12, the data has been normalized to the intensity acquired at 0 Gy. This configuration will continue for the remaining figures.

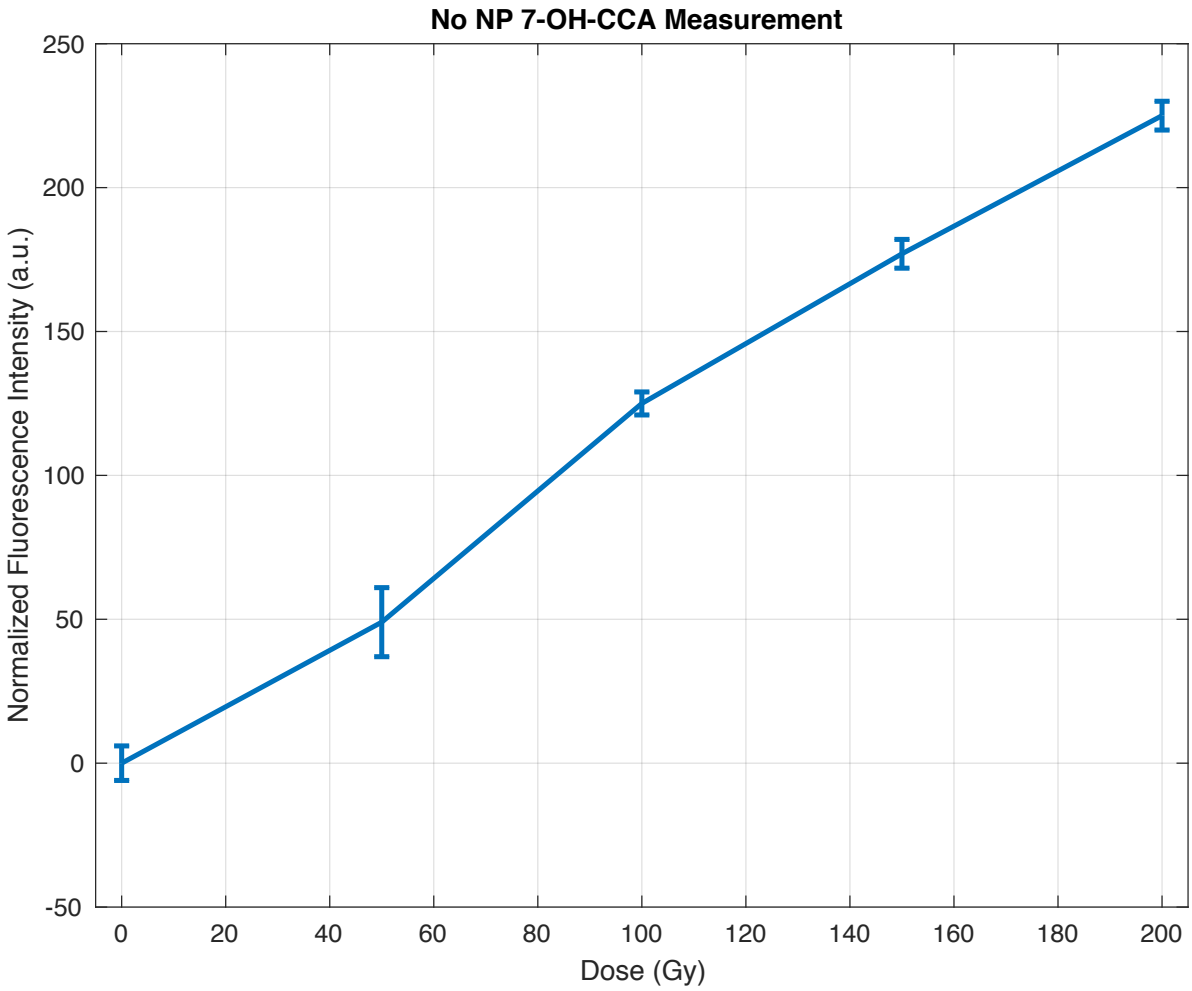

Figure 12.) Fluorescence measurement of 7-OH-CCA of 0.5mM coumarin-3-carboxylic acid irradiated with no nanoparticles.

25nm AuNPs and 3-CCA Irradiated

25nm AuNPs were irradiated using two different concentrations to demonstrate an enhancement of hydroxyl radical production and increased amount of 7-hydroxycoumarin-3-carboxylic acid. These two normalized data schemes can be seen in Figure 13 and are compared to the data collected when no nanomaterial was present.

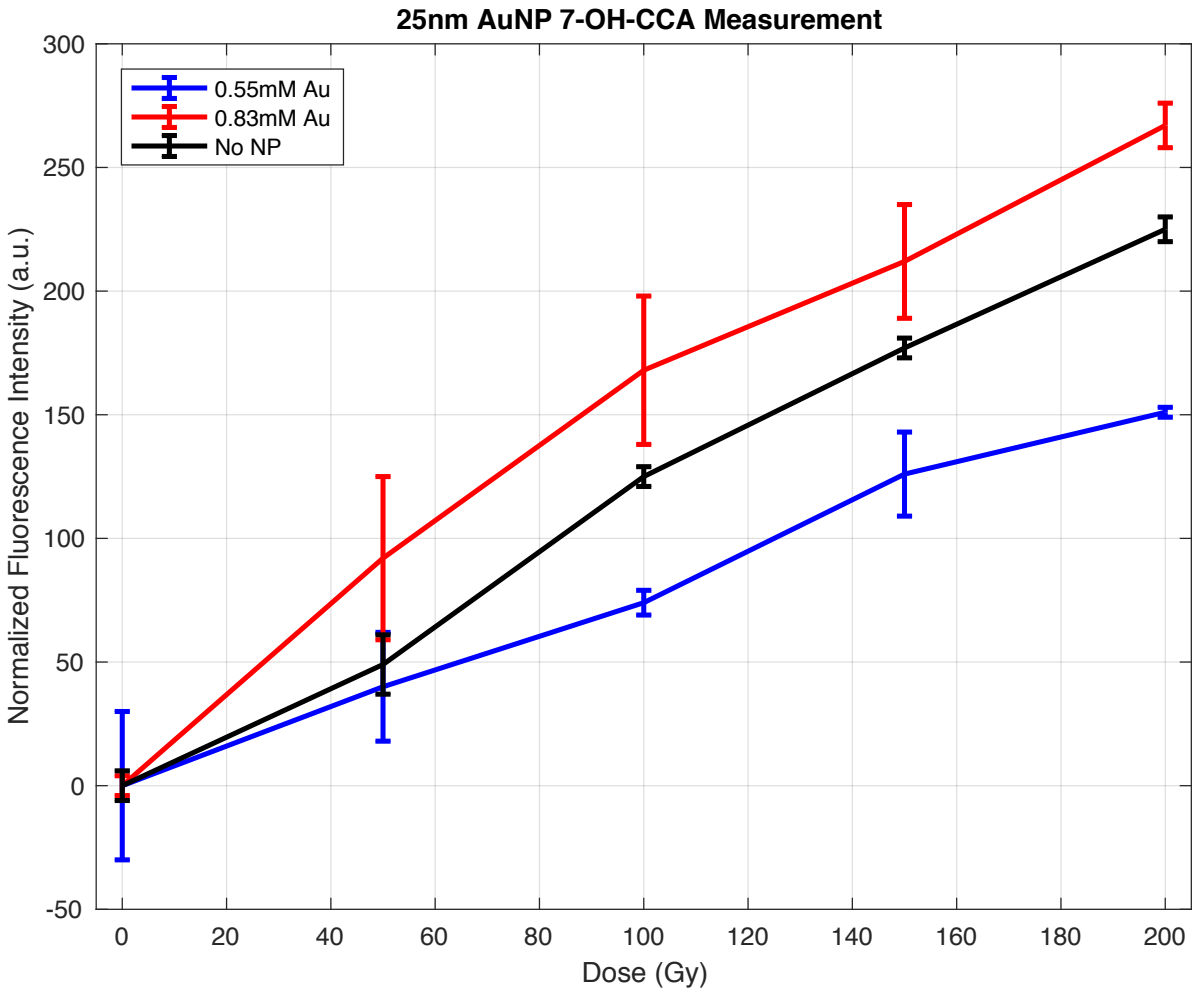

Figure 13.) Fluorescence measurement of 7-OH-CCA of coumarin-3-carboxylic acid irradiated with two varying concentration of 25nm AuNPs, compared to irradiation with no nanoparticles.

Au/$GdVO_4$:Eu NPs with 25nm Au cores and 3-CCA Irradiated

The data for the 25nm AuNPs at two differing concentrations are compared for the fluorescence measurements when the shell was added to the core. Once again these values are measured at the intensity of 447 nm.

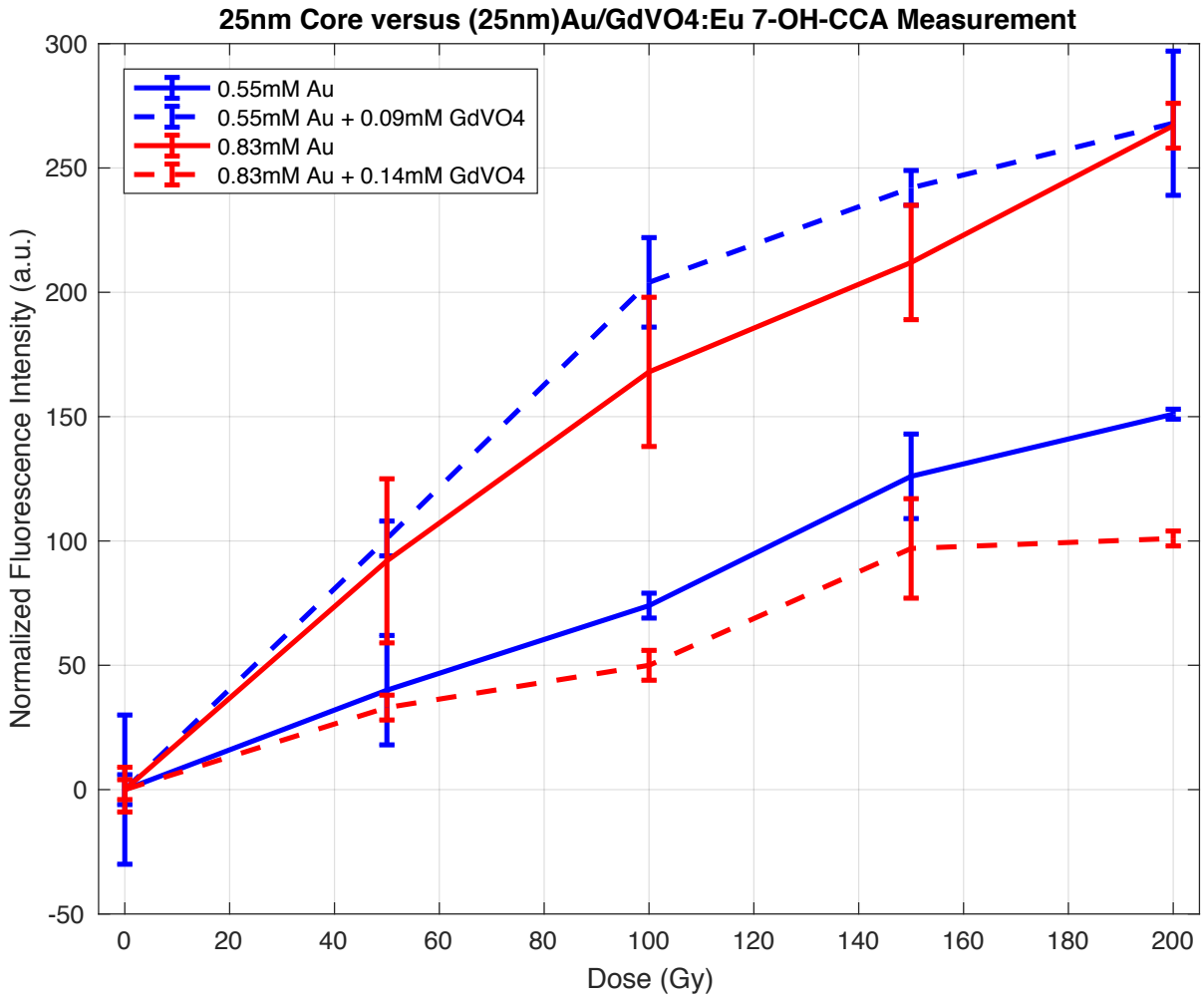

Figure 14.) Comparison fluorescence measurements of 7-OH-CCA in 25nm AuNP irradiated and (25nm)Au/$GdVO_4$:Eu NPs irradiated.

Au/$GdVO_4$:Eu NPs with 12nm Au cores and 3-CCA Irradiated

The fluorescence measurements recorded for the Au/$GdVO_4$:Eu NPs synthesized with the smaller 12 nm cores indicate a mild increase in the fluorescence intensity at higher concentrations. However, as can be seen in Figure 15, most error bars are overlapping except for at a dose of 150 Gy. The intensity at 447 nm is increased slightly for most doses from the lower concentration. Although, as stated, the variation of the measurements is large in this set and must be taken into account.

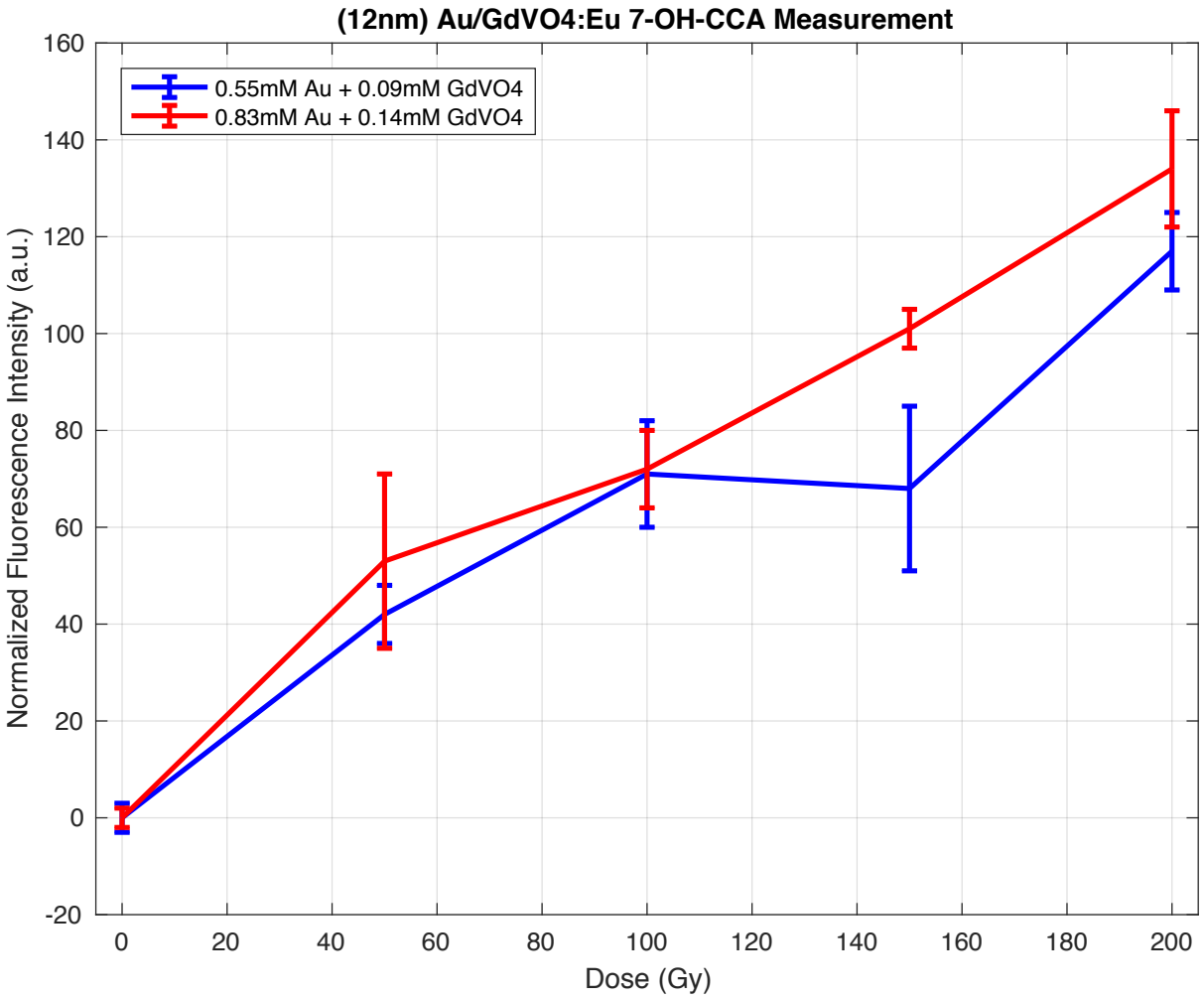

Figure 15.) Fluorescence measurement of 7-OH-CCA of coumarin-3-carboxylic acid irradiated with two varying concentrations of Au/$GdVO_4$:Eu NPs synthesized with 12nm AuNP cores.

7-OH-CCA Estimation

Given the fitted curve for 7-hydroxycoumarin-3-carboxylic acid as obtained and displayed in Figure 11, the equation of y=459x+13.2 was used to estimate the amount of 7-OH-CCA in the samples post irradiation. These are listed in Table I. It should be noted here that the raw data was used for these calculations, not taking into account the quenching effects of the signal.

	7-OH-CCA Estimation (μM)						
Dose (Gy)	No NP	0.55mM 25nm AuNPs	0.83mM 25nm AuNPs	0.55mM Au 12nm cores + 0.09mM GdVO4	0.83mM Au 12nm cores + 0.14mM GdVO4	0.55mM Au 25nm cores + 0.09mM GdVO4	0.83mM Au 25nm cores + 0.14mM GdVO4
0	0.25	0.15	0.075	0	0	0.0060	0.012
50	0.35	0.24	0.28	0.082	0.0098	0.23	0.084
100	0.52	0.31	0.44	0.14	0.16	0.45	0.12
150	0.63	0.42	0.53	0.14	0.22	0.53	0.23
200	0.74	0.48	0.66	0.25	0.29	0.59	0.23

Table I. 7-hydroxycoumarin-3-carboxylic acid estimations within samples following irradiation.

These calculated values seen in Table I bring insight to the amount of 7-hydroxycoumarin-3-carboxylic acid present in the sample immediately following irradiation. This therefore gives an indication of the hydroxyl radical production and whether that has increased in the presence of nanomaterial. Previous groups have reported the fluorescence yield of 7-hydroxycoumarin-3-carboxylic acid to be approximately 3-5%[9][10]. For example, if a 4% yield is found, then for every 100 hydroxyl radicals set forth, 4 will hydroxylate the coumarin-3-carboxylic acid to produce the fluorescent product of 7-hydroxycoumarin-3-carboxylic acid.

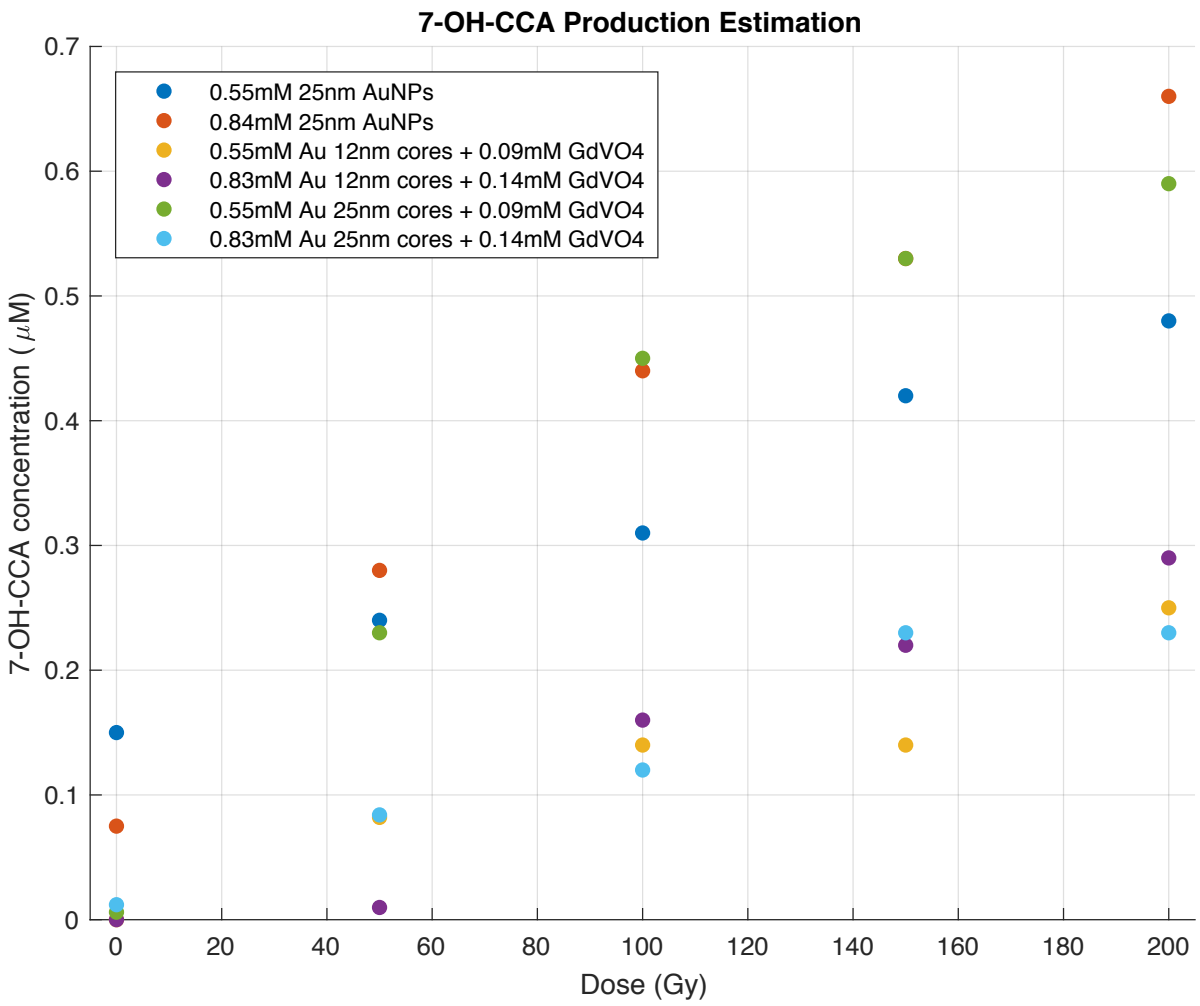

Figure 16.) Comparison of estimations of 7-OH-CCA present in samples post-irradiation.

VI. Discussion

25nm AuNPs and 3-CCA Irradiated

The molarity of gold within the samples of 25nm AuNPs was calculated to be 1.1mM. When diluted for irradiation with coumarin-3-carboxylic acid the molarity of gold was reduced to 0.55mM and 0.83mM in the different samples. As previously stated, the diluted concentration of coumarin-3-carboxylic acid was kept to 0.5mM. Figure 13 shows the fluorescence measurements at the emission wavelength 447 nm for each sample irradiated. It was observed that the lower concentration of nanoparticle solution was below the sample irradiated with no nanoparticles, even at 0 Gy, indicating a quenching of the signal even without irradiation. However, this

reduction in counts may be due to the extended contact time between the nanoparticles and oxidized coumarin. As stated previously, quenching of measured fluorescence is observed due to the interruption of energy transfer in the presence of nanoparticles. Sicard-Roselli et al. observed signal reduction ranging approximately 10-30% after 16 minutes incubation time depending on dose delivered. A larger decrease was observed at higher doses, of 160 Gy as compared to 80 Gy and 120 Gy[9]. Due to the nature of our irradiation protocol and physical spatial locations of equipment laboratory, our contact time of nanoparticles with the oxidized coumarin was approximately five minutes. The longest irradiation time was 96 seconds, however, 3 minutes of centrifugation was also needed for these particles. Based on this literature and our irradiation protocol, the quenching of the fluorescence signal recorded could be nearly 20%.

However, when comparing the normalized values of the gold concentrations, it can be seen that the higher concentration of gold nanoparticles caused increased fluorescence. This result compares to data in the literature where increased concentrations of the nanomaterial, specifically gold, leads to increased radiosensitization and production of ROS[9]. Sicard-Rosseli et al. used concentrations of 0.5 mM and 2 mM under 20 keV irradiation to demonstrate a respective ~120% increase in the linear fitting of 7-hydroxycoumarin-3-carboxylic acid production. Our results support the evidence for increased 7-OH-CCA production at higher concentrations, even at a different irradiation energy. It is noted that a decrease in fluorescence intensity is seen at the lower concentration of gold. This may be due to scavenging caused by residual sodium citrate or nanoparticles left in the solution, however when the concentration is raised enhancement is unbalancing the scavenging and allowing more intense fluorescence. Other considerations when applying this information to an in vivo study would be to consider the toxicity at high concentrations, clearance time of the material, and biocompatibility.

Au/$GdVO_4$:Eu NPs with 25nm Au cores and 3-CCA Irradiated

Figure 14 shows the data collected for both 25nm AuNPs and (25nm)Au/$GdVO_4$:Eu irradiated. This comparison demonstrates the effect of the shell built onto the gold core. There are apparent differences between the less concentrated 0.55mM Au NPs and its equivalent sample with shells as well as the more concentrated samples. The intensity of the more concentrated core/shell sample is dramatically lower than the other core/shell sample. While the shell seems to provide enhancement at the lower concentration, it seems to decrease fluorescence

intensity at the higher concentration. This finding is significant because it allows conclusions to be drawn about the impact of material amounts on enhancement. This could even lead to a concept known as radioprotection.

Radioprotection involves the inactivation of oxide molecules. Nanoparticles can act as mediators during redox reactions, specifically at electron transfer. Recombination as well as neutralization of ROS can occur in the immediate vicinity of nanoparticles, effectively suppressing the damaging effects of the oxide radicals. Orthovanadates and cerium dioxide nanorods have been investigated as radioprotectors and demonstrated their ability to protect tissues and cells from radiation injury[29]. It is important to note the differences in these materials in terms of geometry and composition. The addition of the $GdVO_4$:Eu flower shell on the spherical gold core may be neutralizing more ROS produced due to the core itself and therefore reducing hydroxylation of the coumarin. This is specifically exhibited when higher concentrations of shell material are present. The addition of the gold core at lower concentrations may still allow for the interactions previously described to occur, even with the presence of the shell as to not scavenge the ROS. The production of ROS is likely higher than the scavenging rate of the shell. The lower concentration of the nanomaterial showing increased fluorescence in the presence of the shell may validate the material as enhancing at lower concentrations, and aid in identifying a threshold between the two effects. This concentration dependence has been published before by Hubenko et al., with less production of 7-hydroxucoumarin-3-carboxylic acid when more material was in the aqueous solution. Their work with $GdVO_4:Eu^{3+}$ demonstrated, likely for the first time, the potential for vanadate based nanoparticles to be used as radioprotectors and act as scavengers for ROS, specifically hydroxyl radicals[30]. Previously, cerium oxide materials have been the subject matter for radioprotection.

When comparing the performance of the shells to each other, as represented by the dashed lines in Figure 14, there is significant reduction in the measured signal. We believe this corroborates the findings by Hubenko et al. and supports that with increasing concentrations of $GdVO_4$ present in an irradiated sample, the neutralization of radicals can occur and therefore induce a radioprotectant effect. Despite the synthesized material in this project containing the material of gold at its core, which has established its dosimetric advantages, the orthovanadate present will shield those effects. While this was an unexpected finding of the project, its appearance is very useful and impactful for future endeavors.

Au/$GdVO_4$:Eu NPs with 12nm Au cores and 3-CCA Irradiated

The performance of the Au/$GdVO_4$:Eu NPs synthesized with 12 nm AuNP cores can be seen in Figure 15. There is a small enhancement that can be seen in the fluorescence measurements between the concentrations of the nanomaterial is irradiated. However, it is important to note the overlapping error bars for the majority of the doses administered. This indication of the measured values falling within the standard deviation for each dose makes it difficult to draw any solid conclusions from the data. Therefore evidence of radiosensitization nor radioprotection, also known as "anti-enhancement", can be verified with this portion of the experiments.

Due to the UV-VIS data collected, it is established that these core/shell particles are smaller than that of the core/shells when 25nm AuNPs were utilized. Figure 10 displays this data. Since the same concentrations and amounts of gadolinium nitrate and sodium orthovanadate were used in the shell synthesis despite core size, it can be hypothesized that the shell is thicker on the 12 nm cores. Though these core/shells are not as large in diameter as those with 25 nm cores, the shell accounts for much of the size of the nanoparticle. Due to no significant changes being found in the irradiation data for these particles, one hypothesis could state that thicker shell formation does not contribute to radioprotection and rather it is concentration that is more significant. The crystalline structures of these shells is important to maintain and particularly this flower geometry could be further investigated to solidify its impact.

7-OH-CCA Estimation

The estimations of 7-OH-CCA can be found in Figure 16. In agreement with the literature and manufacturer specifications, the rise in concentration is correlated with the increase in dose administered. Not surprisingly, the highest concentration of AuNPs irradiated revealed the highest amount of 7-OH-CCA consistently amongst most doses, despite being slightly lower at 100 Gy. The lowest production is from the samples of most concentrated (25nm)Au/$GdVO_4$:Eu NPs and less concentrated (12nm)Au/$GdVO_4$:Eu NPs. This corroborates the suspicion of the shell allowing less hydroxylation of the coumarin to form its fluorescent derivative.

VII. Future Work

The introduction of nanomaterial into the medical field has been a work in progress for decades. However, multiple groups have demonstrated synthesis, measurement of radioenhancement, and feasibility in a number of irradiation schema and environments. Due to discrepancies and difficulties comparing previous studies, the transition has been very slow. Cui et al. has made recommendations for future preclinical and clinical trials involving AuNP-based radiosensitization. A standardization for future studies would aid in the clinical transition. Preclinical and in vitro study recommendations include thorough characterization and detailed reporting of physiochemical properties of the material (size, shape, coating, stability, etc.) to be able to correlate with various parameters when using cell lines. The cell lines chosen also allow investigation into the effect of AuNP-based radiosensitization and DNA repair capacity and intrinsic radiosensitvity of the cell line. Considerations for clinical studies include small AuNPs for tumor penetration and distribution, surface coating for stability and uptake, administration routes, and locally advanced tumor types[1]. Nanoparticles of various elemental composition have even been suggested for image-guided external beam radiotherapy, internal radionuclide theranostics, and concomitant therapy with chemotherapy[5].

While many avenues could be taken to investigate multitudes of nanomaterial and enhancement of free radical production, a focus on the current material would be beneficial and allow further descriptions of its behaviors. Future work on the radiosensitization of Au/$GdVO_4$:Eu NPs would include **(i)** irradiating the nanomaterial in the megavoltage range via a linear accelerator, **(ii)** explicitly exploring the behavior of the material in clinical CT and MRI settings, **(iii)** manipulating key characteristics of the NPs for advantageous gain, **(iv)** eventually placing the material in a cell line when deemed feasible and safe, **(v)** the use of different detection probes. Other characterization techniques could also be employed includes the use of transmission electron microscopy (TEM) to have a detailed visual of the material's morphology.

i. MV energy

Placing the nanomaterial under clinically relevant energies and dose rates would be crucial in classifying Au/$GdVO_4$:Eu NPs as a radiosensitizer, or seeing its converse effect as a radioprotector. Other contributing factors to the success of treatment plans would be fractionation schemes as well as administration routes and biodistribution. Previous studies

conducted under lower energies and dose rates, probably as a result of convenience and immediately available resources, was an important start to establishing nanomaterial's potential. However, if the transition to clinic is ever going to occur then relevant data to radiation oncologists and medical personnel needs to be promising. The current experimental setup with using coumarin as a trapping assay would be problematic in the case of a linear accelerator. Due to the delay between placing the nanomaterial, opening and closing the vault door, and the need of fluorescence detection in close spatial proximity, signals measured would likely be very low due to extended times of nanomaterial contact. However, if using a cell line or animal model, survival fractions could be examined as well as survival rates post-irradiation. Other factors could be explored as well as Au/$GdVO_4$:Eu NPs performance under delivery techniques like IMRT and SBRT as well as its performance on the image guidance system of a linear accelerator.

ii. CT/MRI

To establish the synthesized materials as multifunctional nanoparticles, other imaging besides luminescence platforms must be explored. The purposeful addition of dense, high atomic material for differential photoelectric absorption and enhanced contrast must be placed in a CT protocol and analyzed. Visual and Hounsfield unit (HU) analysis would be an additional characterization of the material. Changes such as silver cores instead of gold could also be possible to analyze a shift in image quality. Accumulation of the material could also be visualized in this manner and allow analysis of distribution within a vessel. The addition of gadolinium in the shell may allow for the material to be used as contrast agent for MRI. However investigation in the presence of magnetic field would be necessary to support this.

iii. Nanomaterial

The flexibility of synthesis and the variations available concerning nanomaterial make it a very adaptable process. Simple adjustments could create various geometries, compositions, sizes, thicknesses, etc. that could be investigated thoroughly. This has often been a source of difficulty when comparing studies due to their inherently different parameters. With the aid of characterization techniques to confirm key features, simple modifications in synthesis protocols could easily produce advantageous changes in the nanomaterial to be investigated further. These

could include elemental composition changes. For example, the bright red fluorescence of europium could be changed to terbium doping for a green emission. The size of the nanomaterial as well as the stability is also important considerations. Changes in core size and shell thickness could be investigated, but the stability of the material, including dissociation, would be crucial to explore. Additionally various concentrations of the material could be explored to record the effect of this on the radiosensitization or radioprotection effect. Whether this is for imaging or therapeutic purposes, the level of nanotoxicity should be regarded as an upper limit.

iv. Cell lines

The selection of cell lines and animal models is important transitional step to clinical transition and implementation. This proof of concept has been demonstrated using AuNPs previously and most commonly using rats as test subjects. Selection of radioresistant tumor cells could investigate the usefulness of this material in future trials to effectively improve the treatment of cancer that struggles to be contained effectively. Also this implementation would allow for further characterization of the material in a biological environment and how it behaves in vivo. A number of tools could be used to quantify the material's effectiveness such as survival fraction and survival rates for various time periods. This would be one of the most important experimental sections to establish whether use in humans is viable.

v. Different probes

While the coumarin assay has been a useful and productive tool for the experiments performed, the method does have weaknesses that could be assisted by other techniques. The issues of signal quenching and poor fluorescence contributes uncertainty to the work. Other fluorescent products could be used with a higher yield to improve spectra. However, other investigative tools are available and have been used in the literature as a means of quantifying radiosensitization. Bacteria has been utilized as a benchmark for effective treatments. The removal of algal blooms like microcystis aeruginosa by irradiation has been reported[31]. If the implementation of nanoparticles could reveal a higher removal rate, this would be an effective quantitative finding. Other materials such as methylene blue have been reported to investigate the degradation and complexes with nanomaterial under irradiation[8][24][30].

This work has many promising directions and areas for opportunity for follow-up. A diligent and thorough examination of nanomaterial is needed to find agreement in the research community about the most effective material to synthesize and apply. Clinical transition is a daunting feat for this subject area and will require the collaboration of material scientists, engineers, radiobiologists, medical physicists, radiation oncologists, and many more. If accomplished, it would bring exciting advances to the world of theranostics. This project is a humble but essential beginning to accomplish viable options for testing in the future for Au/$GdVO_4$:Eu nanoparticles.

List of References

1. Cui L, Her S, Borst GR, Bristow RG, Jaffray DA, Allen C. Radiosensitization by gold nanoparticles: Will they ever make it to the clinic? Radiother Oncol [Internet]. 2017;124(3):344–56. Available from: http://dx.doi.org/10.1016/j.radonc.2017.07.007
2. Mesbahi A. A review on gold nanoparticles radiosensitization effect in radiation therapy of cancer. Reports Pract Oncol Radiother [Internet]. 2010;15(6):176–80. Available from: http://dx.doi.org/10.1016/j.rpor.2010.09.001
3. Kim JH, Jenrow KA, Brown SL. Mechanisms of radiation-induced normal tissue toxicity and implications for future clinical trials. Radiat Oncol J. 2014;32(3):103–15.
4. Cooper DR, Bekah D, Nadeau JL. Gold nanoparticles and their alternatives for radiation therapy enhancement. Front Chem. 2014;2(OCT):1–13.
5. Kuncic Z, Lacombe S. Nanoparticle radio-enhancement: Principles, progress and application to cancer treatment. Vol. 63, Physics in Medicine and Biology. Institute of Physics Publishing; 2018.
6. To I, Physics R, Dosimetry R. Gamma- and. 2004;124–59.
7. Gilles M, Brun E, Sicard-Roselli C. Quantification of hydroxyl radicals and solvated electrons produced by irradiated gold nanoparticles suggests a crucial role of interfacial water. J Colloid Interface Sci [Internet]. 2018;525:31–8. Available from: https://doi.org/10.1016/j.jcis.2018.04.017
8. Molina Higgins MC, Clifford DM, Rojas J V. Au@TiO 2 nanocomposites synthesized by X-ray radiolysis as potential radiosensitizers. Appl Surf Sci [Internet]. 2018;427:702–10. Available from: https://doi.org/10.1016/j.apsusc.2017.08.094
9. Sicard-Roselli C, Brun E, Gilles M, Baldacchino G, Kelsey C, McQuaid H, et al. A new mechanism for hydroxyl radical production in irradiated nanoparticle solutions. Small. 2014;10(16):3338–46.
10. Newton GL, Milligan JR. Fluorescence detection of hydroxyl radicals. Radiat Phys Chem. 2006;75(4):473–8.
11. Chen M, Wang JH, Luo ZJ, Cheng ZQ, Zhang YF, Yu XF, et al. Facile synthesis of flower-shaped Au/GdVO4:Eu core/shell nanoparticles by using citrate as stabilizer and complexing agent. RSC Adv. 2016;6(12):9612–8.
12. Escudero A, Becerro AI, Carrillo-Carrión C, Núñez NO, Zyuzin M V., Laguna M, et al.

Rare earth based nanostructured materials: Synthesis, functionalization, properties and bioimaging and biosensing applications. Nanophotonics. 2017;6(5):881–921.

13. Hainfeld JF, Slatkin DN, Smilowitz HM. The use of gold nanoparticles to enhance radiotherapy in mice. Phys Med Biol. 2004;49(18).
14. Hainfeld JF, Smilowitz HM, O'connor MJ, Dilmanian FA, Slatkin DN. Gold nanoparticle imaging and radiotherapy of brain tumors in mice. Nanomedicine. 2013;8(10):1601–9.
15. Al Zaki A, Joh D, Cheng Z, De Barros ALB, Kao G, Dorsey J, et al. Gold-loaded polymeric micelles for computed tomography-guided radiation therapy treatment and radiosensitization. ACS Nano. 2014;8(1):104–12.
16. Miladi I, Alric C, Dufort S, Mowat P, Dutour A, Mandon C, et al. The in vivo radiosensitizing effect of gold nanoparticles based mri contrast agents. Small. 2014;10(6):1116–24.
17. McQuade C, Al Zaki A, Desai Y, Vido M, Sakhuja T, Cheng Z, et al. A multifunctional nanoplatform for imaging, radiotherapy, and the prediction of therapeutic response. Small. 2015;11(7):834–43.
18. Kim JK, Seo SJ, Kim HT, Kim KH, Chung MH, Kim KR, et al. Enhanced proton treatment in mouse tumors through proton irradiated nanoradiator effects on metallic nanoparticles. Phys Med Biol. 2012;57(24):8309–23.
19. Kim JK, Seo SJ, Kim KH, Kim TJ, Chung MH, Kim KR, et al. Therapeutic application of metallic nanoparticles combined with particle-induced x-ray emission effect. Nanotechnology. 2010;21(42).
20. Khadem Abolfazli M, Mahdavi SR, Ataei G. Studying effects of gold nanoparticle on dose enhancement in megavoltage radiation. J Biomed Phys Eng. 2015;5(4):185–90.
21. Náfrádi M, Farkas L, Alapi T, Hernádi K, Kovács K, Wojnárovits L, et al. Application of coumarin and coumarin-3-carboxylic acid for the determination of hydroxyl radicals during different advanced oxidation processes. Radiat Phys Chem [Internet]. 2020;170(September 2019):108610. Available from: https://doi.org/10.1016/j.radphyschem.2019.108610
22. Guo T. Physical, chemical and biological enhancement in X-ray nanochemistry. Phys Chem Chem Phys. 2019;21(29):15917–31.
23. Cheng NN, Starkewolf Z, Davidson RA, Sharmah A, Lee C, Lien J, et al. Chemical

enhancement by nanomaterials under X-ray irradiation. J Am Chem Soc. 2012;134(4):1950–3.

24. Molina Higgins MC, Rojas J V. X-ray radiation enhancement of gold- TiO 2 nanocomposites. Appl Surf Sci. 2019;480(February):1147–55.
25. Rosa S, Connolly C, Schettino G, Butterworth KT, Prise KM. Biological mechanisms of gold nanoparticle radiosensitization. Cancer Nanotechnol. 2017;8(1).
26. Gadoue SM, Toomeh D. Enhancement of linear energy transfer in gold nanoparticles mediated radiation therapy. Phys Medica [Internet]. 2019;60(February):22–9. Available from: https://doi.org/10.1016/j.ejmp.2019.02.019
27. Turkevich J, Stevenson PC, Hillier J. A study of the nucleation and growth processes in the synthesis of colloidal gold. Discuss Faraday Soc. 1951;11(c):55–75.
28. Gilles M, Brun E, Sicard-Roselli C. Gold nanoparticles functionalization notably decreases radiosensitization through hydroxyl radical production under ionizing radiation. Colloids Surfaces B Biointerfaces. 2014;123:770–7.
29. Starodub MF. Nanomaterials for Security. 2016;(January):281–8. Available from: http://link.springer.com/10.1007/978-94-017-7593-9
30. Hubenko K, Yefimova S, Tkacheva T, Maksimchuk P, Borovoy I, Klochkov V, et al. Reactive oxygen species generation in aqueous solutions containing GdVO4:Eu3+ nanoparticles and their complexes with methylene blue. Nanoscale Res Lett. 2018;13.
31. Zheng B, Zheng Z, Zhang J, Luo X, Liu Q, Wang J, et al. The removal of Microcystis aeruginosa in water by gamma-ray irradiation. Sep Purif Technol [Internet]. 2012;85:165–70. Available from: http://dx.doi.org/10.1016/j.seppur.2011.10.005